Unraveling the Role of Ctla-4 in Intestinal Immune Homeostasis: Insights from a novel Zebrafish Model of Inflammatory Bowel Disease

Lulu Qin[a], Chongbin Hu[a], Qiong Zhao[a], Yong Wang[a], Dongdong Fan[a], Aifu Lin[a], Lixin Xiang[a*], Ye Chen[a,c*], Jianzhong Shao[a,b*]

Affiliations:

[a]College of Life Sciences, Key Laboratory for Cell and Gene Engineering of Zhejiang Province, Zhejiang University, Hangzhou, China.

[b]Laboratory for Marine Biology and Biotechnology, Qingdao National Laboratory for Marine Science and Technology, Qingdao, China

[c]Department of Genetic and Metabolic Disease, the Children's Hospital, Zhejiang University School of Medicine, National Clinical Research Center for Child Health, Hangzhou 310052, China.

[*]Corresponding authors: shaojz@zju.edu.cn, yechency@zju.edu.cn, and xianglx@zju.edu.cn

Address correspondence and reprint requests to Prof. Jianzhong Shao, Prof. Ye Chen, and Assoc. Prof. Lixin Xiang, College of Life Sciences, Zhejiang University, 866 YuHangTang Road, Hangzhou 310058, China. Tel.: +86 (571) 88206582; Fax: +86 (571) 88206582.

E-mail addresses: shaojz@zju.edu.cn (J.-z.S.), yechency@zju.edu.cn (Y.C), and xianglx@zju.edu.cn (L.-x.X.)

Abstract

Inflammatory bowel disease (IBD) is a chronic and relapsing immune-mediated disorder characterized by intestinal inflammation and epithelial injury. The underlying causes of IBD are not fully understood, but genetic factors have implicated in genome-wide association studies, including CTLA-4, an essential negative regulator of T cell activation. However, establishing a direct link between CTLA-4 and IBD has been challenging due to the early lethality of CTLA-4 knockout mice. In this study, we identified zebrafish Ctla-4 homolog and investigated its role in maintaining intestinal immune homeostasis by generating a Ctla-4-deficient (*ctla-4*$^{-/-}$) zebrafish line. These mutant zebrafish exhibited reduced weight, along with impaired epithelial barrier integrity and lymphocytic infiltration in their intestines. Transcriptomics analysis revealed upregulation of inflammation-related genes, disturbing immune system homeostasis. Moreover, single-cell RNA-sequencing analysis indicated increased Th2 cells and interleukin 13 expression, along with decreased innate lymphoid cells and upregulated proinflammatory cytokines. Additionally, Ctla-4-deficient zebrafish exhibited reduced diversity and an altered composition of the intestinal microbiota. All these phenotypes closely resemble those found in mammalian IBD. Lastly, supplementation with Ctla-4-Ig successfully alleviated intestinal inflammation in these mutants. Altogether, our findings demonstrate the pivotal role of Ctla-4 in maintaining intestinal homeostasis. Additionally, they offer substantial evidence linking CTLA-4 to IBD and establish a novel zebrafish model for investigating both the pathogenesis and potential treatments.

Key words: Ctla-4 deficiency; inflammatory bowel disease; molecular and cellular mechanisms; zebrafish model

Introduction

Inflammatory bowel disease (IBD), including Crohn's disease and ulcerative colitis, refers to a group of chronic relapsing inflammation disorders affecting the gastrointestinal tract, that have been increasing in prevalence worldwide [1]. The precise etiology of IBD has yet to be fully elucidated. Conventional epidemiological studies have indicated that IBD tends to run in families and is linked to genetic factors [2, 3]. However, research also suggested that susceptibility gene patterns differ significantly among various geographic populations. Current evidence points towards a complicated interaction involving host genetics, disrupted intestinal microbiota, environmental triggers, and abnormal immune responses [4-6]. Advances in genomic sequencing techniques have allowed for the identification of genetic variants associated with an increased risk of developing IBD. Among these, mutations in immune-related genes have received particular attention. Research on humans with Crohn's disease and mouse models of IBD has shown that genetically susceptible individuals exhibit defects in intracellular pattern-recognition receptors (PRRS), such as toll-like receptors (TLR) and nucleotide-binding oligomerization domain (NOD)-like receptors (NLRs), which are responsible for initiating innate immune responses to eliminate harmful bacteria [7, 8]. Genetic variations in the tumor necrosis factor ligand superfamily member 15 (TNFSF15) and interleukin 23 receptor (IL23R) genes, both involved in suppressing

inflammation, have been associated with an increased risk of developing Crohn's disease [9, 10].

Cytotoxic T lymphocyte antigen-4 (CTLA-4), also known as CD152, is one of the most well-established immune checkpoint molecules expressed predominantly on T cells [11-13]. It primarily regulates the early stages of T-cell activation by attenuating downstream signaling of the T cell receptor (TCR) [14-16]. Specifically, CTLA-4 has a much higher affinity for CD80 and CD86 ligands compared to the co-stimulatory receptor CD28 [17, 18]. By outcompeting CD28 for ligand binding, CTLA-4 provides an inhibitory signal that impacts immunological synapse formation and inhibits T-cell proliferation and activation [16, 19]. The immunomodulatory role of CTLA-4 in maintaining immune homeostasis is highlighted through CTLA-4 knockout studies. Germline CTLA-4-deficient is lethal for mice within 3 to 4 weeks due to massive T lymphocyte proliferation and the release of inflammatory cytokines [20-22]. Compared to wild-type T lymphocytes, CTLA-4-deficient T lymphocytes exhibit accelerated development of Th2 cells, leading to significantly enhanced secretion of IL-4 and IL-5 [23, 24]. Additionally, conditional deletion of CTLA-4 in adult mice results in rapid immune activation, multiorgan lymphocyte infiltration, and autoantibody production [25]. Moreover, a selective deficiency of CTLA-4 in Treg cells is sufficient to induce lymphoproliferation and autoimmune diseases in mice [26]. Similarly, associations between polymorphic alleles of CTLA-4 and IBD in humans have been reported in multiple studies [27-29]. Moreover, CTLA-4 is an intriguing target for novel immune checkpoint blockade therapies in cancer treatment, while intestinal inflammation is a

common side effect in these clinical trials [30, 31]. Establishing a direct causal relationship between CTLA-4 and IBD has been challenging due to difficulties in finding appropriate models. The early lethality observed in CTLA-4-deficient mice added another layer of complexity to this issue. Zebrafish is a powerful model system for immunological and biomedical research, due to its versatility and high degree of conservation in innate and adaptive immunities [32, 33]. In our current study, we identified the Ctla-4 homology in zebrafish and successfully developed an adult vertebrate model with homozygous knockout of the *ctla-4* gene for the first time. These *ctla-4*-deficient (*ctla-4*$^{-/-}$) zebrafish survive but exhibit attenuated growth and weight loss. Notably, *ctla-4* deficiency leads to an IBD-like phenotype in zebrafish characterized by altered intestinal epithelial cells morphology, abnormal inflammatory response, defects in microbial stratification and composition. Mechanistically, Ctla-4 exerts its inhibitory function by competing with Cd28 for binding to Cd80/86. These findings establish the *ctla-4* knockout zebrafish as an innovative platform to elucidate CTLA-4 immunobiology, model human IBD, and develop novel therapeutic modalities.

Results

Identification of zebrafish Ctla-4

Through a homology search in the NCBI database, we identified the *ctla-4* gene (XM_005167519.4) on zebrafish chromosome 9, which exhibits an exon organization comparable to that of the human CTLA-4 gene (Fig. S1A-C). Zebrafish Ctla-4 is predicted to be a type I transmembrane protein with a molecular weight of

approximately 33 kDa, featuring structural characteristics of the immunoglobulin superfamily, which include an N-terminal signal peptide, a single IgV-like extracellular domain, a transmembrane region, and a cytoplasmic tail (Fig. 1A). Multiple amino acid sequence alignments revealed that Ctla-4 contains a ^{113}LFPPPY^{118} motif within the ectodomain and a tyrosine-based ^{206}YVKF^{209} motif in the distal C-terminal region (Fig. 1A). These motifs closely resemble the MYPPPY and YVKM motifs found in mammalian CTLA-4 homologs, which are essential for binding to CD80/CD86 ligands, as well as molecular internalization and signaling inhibition [14, 34, 35]. The IgV-like domain of Ctla-4 was characterized by two-layer β-sandwich and was conserved between zebrafish and humans (Fig. 1B). In contrast, zebrafish Cd28 features a SYPPPF motif in its extracellular region and a FYIQ motif in its intracellular tail, distinguishing it from Ctla-4. Additionally, zebrafish Ctla-4, similar to its counterparts in other species, carries a conserved extracellular ^{123}GNGT^{126} motif, which is absent in zebrafish Cd28 [36]. This structural distinction further differentiates Ctla-4 from Cd28 (Fig.1A, Fig. S1D). Consistent with this, phylogenetic analysis showed that Ctla-4 clusters with other known CTLA-4 homologs from different species with high bootstrap probability, whereas zebrafish Cd28 groups separately with other CD28s (Fig. S1C). Structurally, Ctla-4 exists as a dimer, and unlike the intracellular localization of CTLA-4 in mammals, Ctla-4 is found on the cell membrane (Fig. 1C and D). By analyzing the splenic scRNA-seq dataset we recently established [37], Ctla-4 was primarily expressed on the T cells, including the Cd4$^+$ T and Cd8$^+$ T cells (Fig. 1E). This result was verified by immunofluorescence assays on the splenic leukocytes (Fig. 1F).

Ctla-4 deficiency induces inflammatory bowel disease (IBD)-like phenotype

To further investigate the function of Ctla-4, we generated a *ctla-4*$^{-/-}$ zebrafish line with a 14-base deletion in the second exon of the *ctla-4* gene (Fig. 2A-C). The zebrafish appeared grossly normal in appearance; however, the body weight and size were significantly reduced compared with those of wild-type zebrafish (Fig. 2D and E). Anatomically, the *ctla-4*$^{-/-}$ zebrafish were featured by intestine shortening and splenomegaly, suggesting the occurrence of chronic inflammation in the intestines (Fig. 2F and G). For clarification, we first performed histological analysis on the anterior, mid, and posterior intestine segments using H&E staining. Compared to the wild-type zebrafish, the *ctla-4*$^{-/-}$ fish exhibited significant epithelial hyperplasia in the anterior intestine segment, accompanied with a small amount of mucosal inflammatory cell infiltration (Fig. 2H). Moreover, a noteworthy goblet cell loss, reduction of normal mucins and the accumulation of acidic mucins were also observed in *ctla-4*$^{-/-}$ anterior intestine, as detected through Alcian Blue and Periodic Acid-Schiff (AB-PAS) or PAS staining (Fig. 2I and J, Fig. S3A). A small amount of lymphocytic infiltration and mild epithelial damage occurred in the mid intestine segment of *ctla-4*$^{-/-}$ zebrafish (Fig. 2H). In posterior intestine of *ctla-4*$^{-/-}$ fish, the intestinal villi were markedly shortened, the epithelial barrier showed severely disrupted, and the intestinal wall became thinner, wherein the mucosal and transmural inflammatory cells were significantly infiltrated (Fig. 2H). Notably, the intestinal lumens in all three intestinal segments were enlarged in the ctla-4$^{-/-}$ zebrafish, and the ratio between the length of the intestinal villi and the intestinal ring radius was higher in the ctla-4$^{-/-}$ zebrafish intestines compared to those

in wild-type zebrafish (Figure S3B). In addition, the ultrastructure analysis revealed that the epithelial cells of posterior intestine in *ctla-4*$^{-/-}$ zebrafish exhibited alteration in tight junction, the loss of adhesion junctions and desmosomes, and disruption of microvilli (Fig. 2K). All these results strongly indicate that Ctla-4 plays a crucial role in preserving intestinal homeostasis in zebrafish. The intestinal phenotype resulting from Ctla-4 deficiency was similar to IBD in mammals.

Molecular mechanisms of Ctla-4 deficiency-induced IBD-like phenotype

To explore the potential molecular mechanisms of Ctla-4 deficiency-induced IBD-like phenotype, we performed transcriptome profiling analysis of intestines from wild-type and *ctla-4*$^{-/-}$ zebrafish. We identified a total of 1,140 differentially expressed genes (DEGs), among which 714 genes were up-regulated, and 426 genes were down-regulated in *ctla-4*$^{-/-}$ zebrafish (Fig. 3A and B). GO enrichment analysis showed that DEGs or up-regulated genes in the top 10 enriched biological processes were associated with the immune response and inflammatory response (Fig. 3C and D). Moreover, the KEGG enrichment analyses indicated that the up-regulated DEGs are primarily involved in the process of cytokine-cytokine receptor interaction and cell adhesion molecules, which are also related to inflammation (Fig. S4A); however, the down-regulated DEGs were significantly enriched in the process of metabolism (Fig. S4B). The intestines of *ctla-4*$^{-/-}$ zebrafish showed significant upregulation of *il1b*, *tnfa*, myeloid-specific peroxidase (*mpx*), matrix metallopeptidase 9 (*mmp9*), chemokine (C-X-C motif) ligand 8a (*cxcl8a*), and *il13*. In contrast, *il10*, a potent anti-inflammatory cytokine, was markedly down-regulated in Ctla-4-deficient intestines (Fig. 3E). The

transcriptional change of these genes was confirmed by RT-qPCR (Fig. 3F). By constructing the protein-protein interaction (PPI) network, we found that *il1b* was a major cytokine that played a hub role in promoting the bowel inflammation of *ctla-4*$^{-/-}$ zebrafish (Fig. 3G). Moreover, Gene set enrichment analysis (GSEA) showed that genes involved in the lymphocyte chemotaxis, positive regulation of ERK1 and ERK2 cascade, Calcium and MAPK signaling pathways were positively enriched in *ctla-4*$^{-/-}$ zebrafish intestines, implying a sensitized or activated state of lymphocytes due to the absence of Ctla-4 (Fig. S4C and D). Notably, biological processes related to neutrophil activation and chemotaxis were significantly enriched (Fig. 3C and D). Studies have shown that neutrophils can induce histopathological effects through releasing matrix metalloproteinases (MMPs), neutrophil elastase, and myeloperoxidase (MPO) [38]. To confirm the association between neutrophils and Ctla-4-deficient intestinal inflammation, the MPO level was examined. As a support, MPO activity was markedly increased in the intestines and peripheral blood of *ctla-4*$^{-/-}$ zebrafish (Fig. 3H). Besides, a number of biological markers or susceptibility genes of IBD observed in mammals, including c-reactive protein 6 (*crp6*), *crp7*, MMPs, haptoglobin, *il23r*, insulin-like growth factor binding protein 1 a (*igfbp1a*), cAMP responsive element modulator b (*cremb*) and lymphocyte specific protein 1 b (*lsp1b*), were highly expressed in the *ctla-4*$^{-/-}$ zebrafish (Fig. 3I and J) [9, 39, 40], suggesting the presence of a conserved molecular network underlying IBD pathogenesis between *ctla-4*$^{-/-}$ zebrafish and mammalian models.

Cellular mechanisms of Ctla-4 deficiency-induced IBD-like phenotype

198 To investigate the cellular mechanisms underlying the IBD-like phenotype
199 induced by Ctla-4 deficiency, we performed scRNA-seq analysis on intestines from
200 wild-type and *ctla-4*$^{-/-}$ zebrafish using the 10× Genomics Chromium platform. We
201 obtained nine discrete clusters from 7,539 cells of wild-type and *ctla-4*$^{-/-}$ zebrafish (Fig.
202 4A). These clusters of cells were classified as enterocytes, enteroendocrine cells,
203 smooth muscle cells, neutrophils, macrophages, B cells, and a group of T/NK/ILC-like
204 cells based on their co-expression of lineage marker genes (Fig. 4B and C, Fig. S6A
205 and B). Due to severe epithelial disruption and inflammatory cell infiltration in *ctla-4*$^{-}$
206 $^{/-}$ zebrafish intestines, we focused on the pathological process and immune reactions in
207 enterocytes and immune cell populations. KEGG analysis showed that apoptotic
208 pathway was highly enriched in enterocytes of *ctla4*$^{-/-}$ zebrafish, suggesting that
209 aberrant apoptosis contributes to the epithelial injury (Fig. S6C). Subsequently, we
210 conducted a TUNEL assay to detect apoptosis in the posterior intestines from both wild-
211 type and *ctla4*$^{-/-}$ zebrafish. The results showed a higher number of apoptotic cells in the
212 intestines of *ctla4*$^{-/-}$ zebrafish (Fig. S6D). Additionally, genes functionally involved in
213 the formation of tight and adhesion junctions, such as *oclna*, *cdh1*, *pcdh1b* and *cldn15a*,
214 were significantly down-regulated in enterocytes of *ctla-4*$^{-/-}$ zebrafish (Fig. 4D),
215 consistent with the pathological observation under electron microscope. Furthermore,
216 inflammation-related genes and pathways were significantly up-regulated and enriched
217 in neutrophils, B cells, and macrophages of *ctla-4*$^{-/-}$ zebrafish, suggesting active
218 inflammatory responses (Fig. 4E-G, Fig. S6E). By sub-clustering analysis, six
219 subpopulations were classified from T/NK/ILC-like cell groups based on their

220 expression with a set of marker genes. These subpopulations include $Cd8^+$ T cells,
221 ILC3-like cells, maturing $Ccr7^{high}$ T cells, NKT-like cells, and two groups of Th2 cells
222 (Fig. 5A-C, Fig. S7A). The abundances of NKT-like and two subsets of Th2 cells were
223 significantly increased in the intestines of *ctla-4*$^{-/-}$ zebrafish (Fig. 5D-F). These findings
224 were further validated by RT-qPCR detection of their corresponding marker genes (Fig.
225 S7B and C). These cells exhibited high expression levels of *il13* (Fig. 5G and H).
226 Specifically, the second subset of Th2 cells was seldom observed in the intestine of
227 wild-type zebrafish, indicating their unique role in the pathogenesis of IBD-like
228 phenotype in *ctla-4*$^{-/-}$ zebrafish (Fig. 5D-F). KEGG analysis of up-regulated genes from
229 *ctla-4*$^{-/-}$ NKT-like and Th2 cells indicated that Ctla-4 deficiency is positively associated
230 with the inflammatory cytokine-cytokine receptor interaction, PPAR, calcium and
231 MAPK signaling pathways, cellular adhesion and mucosal immune responses (Fig. 5I
232 and J, Fig. S7D). Although the abundance of $Cd8^+$ T cells was not significantly changed
233 in Ctla-4-deficient intestines, the inflammatory genes and pathways were up-regulated
234 and enriched in the subset of T cells (Fig. S7E and F). Notably, the proportion of ILC3-
235 like cells was decreased, and they highly expressed *il17a/f1* and *il17a/f3* in the Ctla-4-
236 deficient intestines (Fig. 5D-F, and K). Investigations have consistently reported a
237 substantial decline in the population of ILC3s within the inflamed intestines and IL-
238 17A-secreting ILC3s play a significant role in the development of intestinal
239 inflammation [41-46]. Thus, the reduced ILC3-like cells and increased expression of
240 *il17a/f1* and *il17a/f3* may be responsible for intestinal inflammation induced by Ctla-4
241 deficiency.

Decreased microbiota diversity in *ctla-4*$^{-/-}$ zebrafish intestines

The intestinal microbiota plays a crucial role in host functions such as nutrient acquisition, metabolism, epithelial cell development and immunity. Notably, lower microbiota diversity has consistently been observed in patients with IBD phenotype [47, 48], making it a valuable indicator of host health. Therefore, we further analyzed whether microbes are involved in the Ctla-4-deficiency induced intestinal inflammation. The results revealed a significantly higher number of amplicon sequence variants (ASVs) in wild-type zebrafish intestines, with 730 ASVs unique to the wild-type group and 276 ASVs exclusively found in *ctla-4*$^{-/-}$ group (Fig. 6A). Furthermore, the Shannon index and the Simpson index indicated a decreased microbial diversity in *ctla-4*$^{-/-}$ zebrafish intestines (Fig. 6B) and the Principal Coordinate Analysis (PCoA) using Bray Curtis distance revealed a significant separation in the microbial composition between *ctla-4*$^{-/-}$ group and the wild-type group (Fig. 6C). To gain insights into the microbial community composition, we analyzed the identified microbial populations at the class and family level. Alphaproteobacteria and Gammaproteobacteria were found to be the most prevalent classes. Relative to wild-type group, Ctla-4 deficiency resulted in a significant reduction in Alphaproteobacteria abundance. However, the Gammaproteobacteria, one of the main classes of Gamma-negative pathogenic bacteria expanded under inflammation conditions, was increased, although the change did not reach statistical significance (Fig. 6D and E) [49]. In addition, we observed a decreased relative abundance of short-chain fatty acids (SCFAs)-producing Bacilli and Verrucomicrobiae, the latter of which contributes to glucose homeostasis and intestinal

health (Fig. 6F and G) [50, 51]. Notably, the family-level analysis revealed a notable enrichment of Enterobacteriaceae, overgrowing under host inflammatory conditions, and the Shewanellaceae, serving as the most important secondary or opportunistic pathogens, in *ctla-4*$^{-/-}$ zebrafish (Fig. 6H and I). To identify differentially abundant bacterial taxa between the wild-type and *ctla-4*$^{-/-}$ zebrafish, we conducted Linear discriminant analysis (LDA) effect size (LEfSe). The results showed that several potentially opportunistic pathogens, including Gammaproteobacteria, Enterobacterales, and Aeromonadales were found to be overrepresented in *ctla-4*$^{-/-}$ zebrafish (Fig. 6J). In contrast, Actinobacteriota, Cetobacterium, and Planctomycetota (Planctomycetes) were more abundant in the wild-type zebrafish. These findings strongly indicated an association between Ctla-4 deficiency-induced gut inflammation and dysbiosis, as characterized by decreased microbial diversity, loss of potentially beneficial bacteria, and expansion of pathobionts.

Inhibitory role of Ctla-4 in T cell activation

Given that Ctla-4 is primarily expressed on T cells (Fig. 1E-F), its absence has been shown to induce intestinal immune dysregulation, indicating a crucial role of this molecule as a conserved immune checkpoint in T cell inhibition. Mechanistically, Ctla-4 may inhibit T cell activation by obstructing the Cd80/86-Cd28 costimulatory pathway, a mechanism conserved in mammalian species. To elucidate the regulatory role of Ctla-4 in costimulatory signal-dependent T cell activation, we conducted a series of blockade and activation assays using anti-Ctla-4 antibody, recombinant soluble Ctla-4-Ig (sCtla-4-Ig), sCd28-Ig, and sCd80/86 proteins in a PHA-stimulating and mixed lymphocyte

reaction (MLR) model. In this system, sCtla-4-Ig and sCd28-Ig served as antagonists to block membrane-bound Cd80/86, while sCd80/86 acted as an agonist for membrane-bound Cd28 (Fig. S8A-C). As expected, the proliferation of lymphocytes from *ctla-4*$^{-/-}$ zebrafish was more pronounced compared to wild-type controls, and the addition of sCtla-4-Ig effectively suppressed this proliferation (Fig. 7A and B). These findings indicate that the absence of Ctla-4 leads to enhanced lymphocyte activation, which can be counteracted by sCtla-4 administration, underscoring the inhibitory function of Ctla-4 in T cell regulation. Consistent with these results, blockade of Ctla-4 using anti-Ctla-4 Ab significantly promoted the proliferation of lymphocytes from wild-type zebrafish (Fig. 7C). Furthermore, sCd28-Ig administration inhibited the proliferation of lymphocytes from *ctla-4*$^{-/-}$ zebrafish (Fig. 7D), whereas sCd80/86 promoted the expansion of Ctla-4-deficient lymphocytes (Fig. 7E). Based on these results, we concluded that the presence of Ctla-4 obstructs the Cd80/86-Cd28 mediated costimulatory signaling, consequently impeding cell proliferation. To further investigate the molecular interactions between Cd28, Ctla-4, and Cd80/86, we employed AlphaFold2 to predict the structures of Cd80/86-Cd28 and Cd80/86-Ctla-4 complexes. A total of 25 models were generated for each complex and subsequently aligned with Cd80/86. The predictions indicated that both Cd28 and Ctla-4 form a well-defined interface with Cd80/86, utilizing the same binding site (Fig. S8D and E). This well-defined interface was corroborated by lower predicted aligned error (PAE) scores for each model, as marked by the red dashed square (Fig. 7F and G). Subsequently, co-immunoprecipitation (Co-IP) assays were conducted to provide compelling evidence

for the molecular interactions between Cd80/86 and Cd28 or Ctla-4. Flow cytometry analysis further revealed dose-dependent associations between Cd80/86 and Cd28 or Ctla-4 in HEK293T cells (Fig. 7H, S8F). Additionally, microscale thermophoresis assays demonstrated that Ctla-4 exhibits a higher binding affinity for Cd80/86 than Cd28, as evidenced by a lower equilibrium association constant value ($K_D = 0.50 \pm 0.25$ μM vs. $K_D = 2.64 \pm 0.45$ μM) (Fig. 7I). These findings suggest that Ctla-4 exerts its inhibitory function by competing with Cd28 for binding Cd80/86.

sCtla-4-Ig alleviates IBD-like phenotype

As described above, engagement of Cd80/86 by sCtla-4-Ig effectively suppressed T cell activation *in vitro* (Fig. 7B), indicating that sCtla-4-Ig holds promise as a potential intervention for IBD-like phenotype. This is supported by the observation that Ctla-4-deficient zebrafish treated with sCtla-4-Ig exhibited obvious body weight restoration compared to those treated with the IgG isotype control (Fig. 8A). To provide further evidence, histological analysis was performed on the posterior intestine, which is known to experience severe tissue destruction under Ctla-4 deficient conditions. As expected, Ctla-4-Ig treatment resulted in a significant decrease in lymphocyte infiltration and an improvement in the epithelial barrier (Fig. 8B). Moreover, Ctla-4-Ig treatment significantly reduced the expression of pro-inflammatory genes, including *il13*, *tnfa*, *mpx*, *mmp9*, and *cxcl8a*, as well as *igfbp1a*, *cremb*, and *lsp1a*, which are susceptibility genes for IBD observed in mammals (Fig. 8C and D). These findings demonstrate that the supplementation of Ctla-4-Ig alleviates intestinal inflammation in Ctla-4-deficient zebrafish, highlighting its potential as a therapeutic intervention for

CTLA-4 deficiency-induced IBD in mammals.

Discussion

As an essential negative regulator of T cell activation, dysfunction of CTLA-4 was implicated in various diseases in both humans and murine models [20, 21, 52]. Numerous previous studies have established the connection between CTLA-4 and autoimmune thyroiditis, Graves' disease, myocarditis, pancreatitis, multiple sclerosis, rheumatoid arthritis, and type I diabetes [53-59]. However, the involvement of CTLA-4 in IBD has been understudied. Several investigations have reported that haploinsufficiency resulting from mutations in CTLA-4 in humans is associated with IBD, and genome-wide association studies (GWAS) have implicated CTLA-4 as a susceptibility gene for IBD [60-62]. Nevertheless, the exact contributions and mechanisms of CTLA-4 deficiency in the occurrence and pathology of IBD remain incompletely understood, primarily due to the lack of animal models attributable to the lethality of CTLA-4 knockout in mice. In this study, we identified the Ctla-4 homolog in zebrafish, and discovered that defect in Ctla-4 did not have a severe lethal effect, but did show a clear IBD-like phenotype. This makes zebrafish an attractive animal model for investigating the molecular and cellular mechanisms underlying Ctla-4 mediated IBD.

Multiple lines of histopathological evidence demonstrated the IBD-like phenotype in Ctla-4-deficienct zebrafish. Key features include epithelial hyperplasia, disruption of epithelial integrity, loss of goblet cells, increased acidic mucus production, intestinal

lumen enlargement, inflammatory cell infiltration, and elevated expression of pro-inflammatory cytokines in the inflamed intestines. These characteristics, such as epithelial hyperplasia, goblet cell depletion, inflammatory cell infiltration, and upregulated pro-inflammatory cytokine expression, closely resemble those observed in the dextran sodium sulfate (DSS)-induced IBD model in mice [63]. Similarly, mononuclear cell infiltration and significant upregulation of the il1β cytokine have been reported in the trinitrobenzenesulfonic acid (TNBS)-induced IBD model in adult zebrafish [64]. In zebrafish larvae, the TNBS-induced IBD-like phenotype also exhibits an enlarged intestinal lumen, although goblet cell numbers were increased [65]. Additionally, neutrophilic inflammation and acidic mucin accumulation have been observed in the DSS-induced enterocolitis model in zebrafish larvae [66]. In contrast, the soybean meal-induced enteritis (SBMIE) phenotype in zebrafish larvae shows no significant structural changes in intestinal architecture, despite an increased number of neutrophils and lymphocytes [67]. In summary, Ctla-4 deficiency induces IBD-like phenotypes analogous to those typically elicited by drugs in mice and zebrafish, making this model a valuable tool for comprehending the pathophysiological mechanisms underlying IBD.

A transcriptomics study was conducted to investigate the mechanisms of Ctla-4-deficiency induced IBD. RNA-seq analysis demonstrated a significant upregulation of important inflammatory cytokines, such as *il1b* and *tnfa* in the Ctla-4-deficient intestines. This is consistent with studies showing that IL-1β and TNF-α act as crucial mediators in mammalian IBD models by disrupting epithelial junctions and inducing

374 apoptosis of epithelial cells [68, 69]. Conversely, the key anti-inflammatory cytokines,
375 such as *il10*, were downregulated. These findings highlight an imbalance between pro-
376 inflammatory and anti-inflammatory cytokines in the intestines of Ctla-4-deficient fish.
377 Consistently, the inflammatory signaling pathways associated with these upregulated
378 cytokines, such as the ERK1/2 and MAPK pathways, were positively enriched in
379 inflamed intestines. Single-cell RNA-seq analysis revealed the upregulation and
380 enrichment of these inflammatory cytokines and pathways in neutrophils, macrophages,
381 and B cells of inflamed intestines, indicating their active involvement in inflammatory
382 responses and as major sources of inflammatory signals. Additionally, there was a
383 marked increase in the abundance of Th2 subset cells in the inflamed intestines, these
384 cells exhibited high expression of *il13* and were significantly enriched in inflammatory
385 signaling pathways, indicating their activated state. These findings align with previous
386 studies indicating that T cells in CTLA-4-deficient mice exhibit a bias toward Th2
387 differentiation [23, 24]. Furthermore, IL-13, a key effector Th2 cytokine, has been
388 implicated in the pathogenesis of ulcerative colitis in mammals, where it directly
389 contributes to epithelial cell damage by disrupting tight junctions, inducing apoptosis,
390 and impairing cellular restitution [70]. Therefore, upregulated Il13 from Th2 cells may
391 be a significant contributor to the occurrence of intestine inflammation in Ctla-4-
392 deficient zebrafish. Notably, the proportion of ILC3-like cells was downregulated in the
393 inflamed intestines, consistent with recent studies reporting a substantial decline of
394 ILC3 in IBD patients [41-43]. ILC3 is the most abundant type of ILCs in the intestines
395 and plays a protective role in IBD in mammals by promoting epithelial cell proliferation

and survival, as well as enhancing intestinal barrier function through the production of IL-22 [44, 46]. Thus, the marked decrease in ILC3-like cells may exacerbate intestinal inflammation and damage.

IBD is frequently associated with alterations in gut microbiota composition, characterized by reduced microbial diversity and an imbalance between beneficial and pathogenic bacteria. The common feature of these changes is the expansion of Proteobacteria, particularly members of the Enterobacteriaceae family [71, 72]. Similarly, Ctla-4-deficient zebrafish exhibited significant enrichment of Enterobacteriaceae, alongside a decline in beneficial bacteria like Cetobacterium and an increase in opportunistic pathogens such as γ-Proteobacteria and Aeromonadales. These findings indicate shared patterns in microbial flora changes during intestinal inflammation. Previous studies suggest that reduced microbial diversity in IBD results from the loss of normal anaerobic bacteria, such as Bacteroides, Eubacterium, and Lactobacillus [73]. Concurrently, inflammation-driven increases in intestinal lumen oxygenation and the availability of nitrate and host-derived electron acceptors facilitate anaerobic respiration and Enterobacteriaceae proliferation [74]. These observations highlight the intricate interplay between IBD pathogenesis, gut microbial alterations, and host immune homeostasis. The zebrafish IBD-like model induced by Ctla-4 deficiency offers new insights into this research area. For instance, abnormal activation of Th2 cells may lead to dysfunction in downstream B cells and mucosa-associated immunity, which are crucial for maintaining symbiotic bacterial homeostasis in the intestines [50]. This suggests a potential link between Th2 cell changes and the

observed alterations in the intestinal microbial community in Ctla-4-deficient zebrafish. Moreover, Ctla-4 deficiency alters the proportion and activation of ILC3 cells and damages the intestinal epithelium, potentially shaping the inflammatory milieu and further disrupting gut microbial homeostasis. Ctla-4 also regulates T cell activation by inhibiting the Cd80/86 co-stimulatory pathway. These findings suggest a regulatory interplay between Ctla-4, ILC3 cells, Cd80/86-primed T cells, and gut microbiota in Ctla-4 deficiency-induced IBD. Recently, gut microbiota exposure has been found to induce local IL-23 production, which upregulates CTLA-4 on ILC3s. This supports immune regulation by reducing CD80/86 co-stimulatory signaling and increasing PD-L1 bioavailability on myeloid cells. Impairment of this pathway manifests in a substantial imbalance of effector and regulatory T cell responses, exacerbating intestinal inflammation [75]. These findings bolster our hypothesis and provide valuable insights into the complex interactions between gut microbiota, ILC3-mediated immune responses, and Cd80/86 signaling in Ctla-4 deficiency-induced IBD.

In conclusion, our study demonstrates that Ctla-4 serves as a potential genetic determinant of the IBD-like phenotype in zebrafish, although further research is necessary to conclusively identify the causative variant responsible for this association. The development of this zebrafish model offers a valuable tool for elucidating the mechanisms underlying the disease's pathophysiology. Nevertheless, a deeper understanding of the intricate interactions among immune cells, intestinal epithelial cells, and the microbiome in IBD remains an area warranting further investigation.

Materials and Methods

Experimental fish

The AB strain zebrafish (*Danio rerio*) of both sexes, 4-6 months of age with body weights ranging from 0.3 to 0.8 g and lengths of 3-4 cm, were reared in the laboratory in recirculating water at 26-28 ℃ under standard conditions as previously described [76]. All animal experiments were performed in compliance with legal regulations and approved by the Research Ethics Committee of Zhejiang University. For sampling, wild-type and Ctla-4-deficient zebrafish of varying ages were kept in separate tanks and labeled with their respective dates of birth. Wild-type zebrafish aged 4-6 months and Ctla-4-deficient zebrafish aged 4 months were used for the experiments.

Generation of Ctla-4-deficient zebrafish

CRISPR/Cas9 system was used to knock out the *ctla-4* gene. The targeting sequence 5'-CTCAGAGCCCTACTTCGCAA-3' was designed by optimized CRISPR Design (http://crispr.mit.edu/) and synthesized by T7 RNA polymerase and purified by MEGAclear Kit (AM1908; Invitrogen) *in vitro*. Cas9 protein (500 ng/μl, A45220P; Thermo Fisher Scientific) and purified RNA (90 ng/μl) were coinjected into one cell-stage wild-type embryos. For genotyping, DNA fragment was amplified with primers (F: 5' -TGTGACAGGAAAAGATGGAGAA- 3' and R: 5'-GATCAGATCCACTCCTCCAAAG- 3') at 94℃ for 4 min followed by 35 cycles at 94℃ for 30 s, 58℃ for 30 s and 72℃ for 30 s, culminating in a final extension at 72℃ for 10 min. Subsequently, the PCR product was subjected to sequencing. The mutant alleles (-14 bp) were obtained. As with wild-type zebrafish, Ctla-4-deficient zebrafish

462 were reared in the laboratory in recirculating water at 26-28 ℃ under standard
463 conditions.

464 **Preparation of recombinant proteins**

465 For prokaryotic expression, the encoding sequences for the extracellular domains
466 of Ctla-4 and Cd80/86 (designated as soluble Cd80/86, sCd80/86) were amplified and
467 cloned into the pET-28a (+) and pCold-GST vectors. The primers used are shown in
468 Supplemental Table 1. The recombinant plasmid was transformed into *Escherichia coli*
469 BL21 (DE3) competent cells (TransGen Biotech) and induced with isopropyl-β-D-
470 thiogalactoside (IPTG, 0.5 mM) at 20℃ for 12 h. After ultrasonication, the supernatants
471 were collected for purification. For eukaryotic Ctla-4-Ig and Cd28-Ig expression, the
472 extracellular domains of Ctla-4 and Cd28 were fused to the Fc region of human IgG1
473 [77], and cloned into the pAcGHLTc vector. The recombinant plasmids were transfected
474 into sf9 (*Spodoptera frugiperda*) cells with baculovirus vector DNA (AB Vector) under
475 the assistance of lipofectamine™ 3000 (Thermo Fisher Scientific). The cells were
476 cultured at 28℃ for 3 days and subsequently dissolved in a lysing buffer (50 mM Tris-
477 HCl, pH 8.0, 150 mM NaCl, 1% Nonidet P-40, 1 mM PMSF). The recombinant Ctla-
478 4-Ig and Cd28-Ig proteins (designated as soluble Ctla-4-Ig, sCtla-4-Ig and sCd28-Ig)
479 were purified using Ni-NTA agarose affinity chromatography (QIAGEN) following the
480 manufacturer's protocol. Proteins were then separated on a 12% SDS-PAGE gel and
481 visualized through Coomassie Brilliant Blue R250 staining.

482 **Preparation of polyclonal antibody**

483 Antibody (Ab) against the Ctla-4 extracellular domain protein was produced

484 through a recombinant protein immunized approach as previously described [78].
485 Briefly, four-week-old male BALB/c mice (~15 g) were immunized with recombinant
486 Ctla-4 protein with extracellular domain (25 μg) each time in CFA (Sigma-Aldrich)
487 initially and then in IFA (Sigma-Aldrich) for four times thereafter at biweekly intervals.
488 Seven days after the final immunization, serum samples were collected when anti-
489 serum titers exceeded 1:10,000. The Ab was affinity purified by Protein-A Agarose
490 Columns (Thermo Fisher Scientific), and its titer was examined by ELISA. The validity
491 and specificity of the Ab was determined by Western blot analysis.

492 **Subcellular localization**

493 HEK293T cells were seeded into the 12-well plates (Corning) with cover glass and
494 cultured in high-glucose DMEM (Gibco) supplemented with 10% FBS (Cell-Box) at
495 37°C in 5% CO_2 to allow growth until 40%-50% confluence. The cells were transfected
496 with pEGFPN1-Ctla-4 plasmid DNA (0.8 μg) with the help of PEI reagent (3.2 μg per
497 well) in accordance with the manufacturer's protocol. After transfection for 24 h, the
498 cells were fixed with 4% paraformaldehyde (PFA; Sigma-Aldrich) and stained with
499 CM-DiI (1 μM; Thermo Fisher Scientific) and DAPI (100 ng/ml; Sigma-Aldrich). The
500 fluorescence images were obtained using a two-photon laser scanning confocal
501 microscope (LSM710; Zeiss, Jena, Germany) with ×630 magnification.

502 **Identification of monomer or dimer**

503 HEK293T cells were transfected with pCDNA3.1-HA-Ctla-4 (0.8 μg) or
504 pCDNA3.1-HA (0.8 μg) under the assistance of polyethylenimine (PEI; Sigma-
505 Aldrich). After 48 h, the cells were lysed with precooling cell lysis buffer (Beyotime)

and the supernatants were mixed with non-reducing (without β-ME) or reducing (with β-ME) loading buffer for Western blot analysis.

Immunofluorescence staining

Colocalization of Cd4-1/Cd8α and Ctla-4 was determined by immunofluorescence staining. Leukocytes were isolated from zebrafish's spleen, kidney, and peripheral blood by Ficoll-Hypaque (1.080 g/ml; Sangon Biotech) centrifugation at 2,500 rpm at 25℃ for 25 min. After washing with D-Hank's solution, cells were fixed with 4% PFA at room temperature for 10 min, blocked with 2% BSA (Sigma-Aldrich), and incubated with primary Abs at 4°C for 2 h. The primary Abs included combinations of rabbit anti-CD4-1 and mouse anti-CTLA-4, or rabbit anti-CD8α and mouse anti-CTLA-4, which were produced in our laboratory as previously described [75]. Following another wash with D-Hank's solution, the cells were combined with secondary Abs, including FITC-conjugated goat anti-rabbit IgG and PE-conjugated goat anti-mouse IgG (Thermo Fisher Scientific), according to the manufacturer's instructions. After a final wash with D-Hank's solution, the cells were stained with DAPI (100 ng/ml) at room temperature for 10 min. Fluorescence images were captured using a two-photon laser confocal scanning microscope (LSM710; Zeiss, Jena, Germany) with ×630 magnification.

Myeloperoxidase activity measurement

The myeloperoxidase (MPO) activity in intestine and peripheral blood was quantified using a commercial colorimetric assay kit (Nanjing Jiancheng Bioengineering Institute, China) according to the manufacturer's instructions. Briefly, intestinal tissues were homogenized in extraction buffer to obtain a 5% homogenate,

while peripheral blood was mixed with extraction buffer at a 1:1 ratio. A 180 μl aliquot of resultant mixture was incubated with 20 μl of reaction buffer for 15 min at 37°C. Enzymatic activity was determined by measuring the changes in absorbance at 460 nm using a 96-well plate reader. MPO activity was expressed as units per gram of wet intestinal tissue or per milliliter of peripheral blood.

Co-immunoprecipitation and Western blot analysis

Co-immunoprecipitation (Co-IP) was performed to detect the interaction between Cd28/Ctla-4 and Cd80/86. HEK293T cells were co-transfected with pLVX-mCherry-C1-Cd28 (3 μg) and pEGFP-N1-Cd80/86 (3 μg) or pEGFP-N1-Ctla-4 (3 μg) and pCDNA3.1-HA-Cd80/86 (3 μg) using PEI as a transfection reagent. At 48 h post-transfection, the cells were lysed with pre-cooled cell lysis buffer (Beyotime). The lysates were centrifuged at 12,000 × g for 8 minutes at 4°C, and the supernatants were incubated with mouse anti-myc mAb (Abmart) or mouse anti-HA mAb (Abmart) overnight at 4°C. Expression of the transfected plasmids was analyzed in the whole cell lysates as an input control. The following day, the mixture was incubated with 50 μl of protein A agarose beads (Thermo Fisher Scientific) for 4 h. The beads were washed 3 times with lysis buffer and mixed with loading buffer for SDS-PAGE separation. Target proteins were transferred onto a 0.22-μm polyvinylidene difluoride (PVDF) membrane (EMD Millipore) for Western blot analysis. The blots were blocked with 5% skimmed milk, incubated with mouse or rabbit primary Abs overnight at 4°C, washed with TBST, and then incubated with HRP-conjugated goat anti-mouse/rabbit IgG mAb (Abmart) at room temperature for 1 h. Detection was performed using a gel imaging system (Tanon

4500).

Histopathological analysis

The anterior, mid, and posterior intestines (n = 3 replicates) were fixed in 4% PFA overnight and embedded in paraffin. The tissues were cut into 4 μm sections and stained with hematoxylin and eosin (H&E) for histopathological analysis. To evaluate the severity of intestinal inflammation, histologic scores were determined based on established criteria from a previous study [79]. Briefly, three independent parameters, including inflammation severity, inflammation extent, and epithelial changes, were assessed and scored as follows: inflammation severity (0 = none, 1 = minimal, 2 = mild, 3 = moderate, 4 = marked); inflammation extent (0 = none, 1 = mucosa, 2 = mucosa and submucosa, 3 = transmural), epithelial changes (0 = none, 1 = minimal hyperplasia, 2 = mild hyperplasia, minimal goblet cell loss, 3 = moderate hyperplasia, mild goblet cell loss, 4 = marked hyperplasia with moderate to marked goblet cell loss). Each parameter was calculated and summed to obtain the overall score. Additionally, tissue sections were stained with Periodic Acid-Schiff (PAS) or Alcian Blue and Periodic Acid-Schiff (AB-PAS) reagent to evaluate the mucin components and goblet cell numbers.

Transmission electron microscopy observation

The posterior intestines were cut into 0.2 cm segments and then split lengthwise to expose the intestinal villi to the fixative fully. The samples were first fixed with 2.5% glutaraldehyde in phosphate buffer (0.1 M, pH 7.0) overnight at 4℃, washed three times in the phosphate buffer for 15 min at each step and post-fixed in 1% OsO_4 for 1

572 h. Following gradient acetone dehydration and Spurr resin infiltration (1:1 and 1:3
573 mixture of absolute acetone and the final Spurr resin mixture for 1 h and 3 h, and final
574 Spurr resin mixture overnight), the specimens were placed in Eppendorf contained
575 Spurr resin and heated at 70℃ for overnight. The samples were sectioned using an
576 ultratome (LEICA EM UC7). Then, the sections were stained with uranyl acetate and
577 alkaline lead citrate for 10 min each and observed under a transmission electron
578 microscopy (Hitachi Model H-7650).

579 **Assessment of apoptosis by TUNEL**

580 The posterior intestines were fixed by 4% paraformaldehyde and embedded in
581 paraffin. Apoptosis was detected using TUNEL staining following the manufacturer's
582 protocol (Beyotime). Briefly, deparaffinized sections were incubated with biotin-dUTP
583 labeling solution (TdT Enzyme: Biotin-dUTP = 1: 9) for 1 h, followed by incubation
584 with streptavidin-HRP for 30 min at room temperature. Positive signals were visualized
585 using DAB chromogenic solution and counterstained with hematoxylin. Apoptotic cells
586 and the area of the intestinal epithelium were quantified, and the apoptosis index was
587 calculated as the number of apoptotic cells per 1×10^4 μm^2 observed using ImageJ
588 software.

589 **RNA-sequencing and bioinformatic analysis**

590 Total RNAs were isolated from wild-type or *ctla-4*$^{-/-}$ intestines (three biological
591 replicates) using TRIzol reagent following the manufacturer's instructions (Takara).
592 cDNA libraries were constructed using NEB Next Ultra Directional RNA Library Prep
593 Kit (NEB), and sequencing was performed according to the Illumina Hiseq2500

standard protocol at LC Bio (Hangzhou, China). The differentially expressed genes (DEGs) were identified with absolute Log_2 fold change > 1 and adjusted *p*-value < 0.05 by R package DESeq2. Gene Ontology (GO) enrichment and Kyoto encyclopedia of genes and genomes (KEGG) enrichment analyses were performed by the OmicStudio (http://www.omicstudio.cn/tool) tools. Gene-set enrichment analysis was performed using software GSEA (v4.1.0, https://www.gsea-msigdb.org/gsea/index.jsp), and the heatmap was generated using the R package ggplot2. For the protein-protein interaction (PPI) networks, the DEGs were retrieved in STRING (version 11.5, https://string-db.org/) database (combined score > 0.4), and the PPI network was visualized by Cytoscape software (version 3.9.1) [80]. The betweenness centrality (BC) was calculated using the CytoNCA plugin in Cytoscape software. The RNA-sequencing (RNA-seq) data in this study were deposited in the Gene Expression Omnibus (GEO) (http://www.ncbi.nlm.nih.gov/geo/) database.

Quantitative real-time PCR

The transcript abundance of target genes was quantified using quantitative real-time PCR on a CFX Connect Real-Time PCR Detection System equipped with Precision Melt Analysis™ Software (Bio-Rad, Cat. No. 1855200EM1). Total RNA from intestines was extracted using TRIzol reagent (Takara Bio) and reverse transcribed into cDNAs according to the manufacturer's protocol. PCR experiments were performed in a total volume of 10 μl by using an SYBR Premix Ex Taq kit (Takara Bio). The reaction mixtures were incubated for 2 min at 95°C, then subjected to 40 cycles of 15 s at 95°C, 15 s at 60°C, and 20 s at 72°C. Relative expression levels of the target

616 genes were calculated using the $2^{-\Delta\Delta ct}$ method with β-actin for normalization. Each PCR
617 trial was run in triplicate parallel reactions and repeated three times. The primers used
618 in the experiments are listed in Supplemental Table 1.

619 **Single-cell RNA-sequencing analysis**

620 The intestines from wild-type (30 fish) and *ctla-4*$^{-/-}$ zebrafish (30 fish) were
621 washed by D-Hank's and incubated with D-Hank's containing EDTA (0.37 mg/mL) and
622 DTT (0.14 mg/mL) for 20 min. The resulting supernatants were collected as fraction 1.
623 The remaining tissues were subsequently digested with type IV collagenase (0.15
624 mg/mL) for 1 h at room temperature and the resulting supernatants were collected as
625 fraction 2. Fractions 1 and 2 were combined and centrifuged at 350 g for 10 min. Cells
626 were then washed with D-Hank's and suspended in a 40% Percoll (Shanghai Yes
627 Service Biotech, China) solution (Percoll: FBS: L-15 medium = 4: 1: 5) and passed
628 through a 40-μm strainer (Bioland). The cell suspension was carefully layered onto 63%
629 Percoll (Percoll: FBS: L-15 medium = 6.3: 1: 2.7) and centrifuged at 400 g for 30 min
630 at room temperature. The cell layer at the interface was collected and washed with D-
631 Hank's at 400 g for 10 min. Cell quantity and viability were assessed using 0.4% trypan
632 blue staining, revealing that over 90% of the cells were viable. Single-cell samples
633 (8,047 cells in wild-type group, 8,321 cells in *ctla-4*$^{-/-}$ group) were submitted to the LC-
634 Bio Technology Co., Ltd (Hangzhou, China) for 10× Genomics library preparation and
635 data analysis assistance. Libraries were prepared using the Chromium™ Controller and
636 Chromium™ Single Cell 3' Library & Gel Bead Kit v2 (10× Genomics) according to
637 the manufacturer's protocol, and sequenced on an Illumina NovaSeq 6000 sequencing

system (paired-end multiplexing run, 150 bp) at a minimum depth of 20,000 reads per cell. Sequencing results were demultiplexed and converted to FASTQ format using Illumina bcl2fastq software and the data were aligned to Ensembl zebrafish genome assembly GRCz11. Quality control was performed using the Seurat. DoubletFinder R package was used to identify and filter the doublets (multiplets) [81]. The cells were removed if they expressed fewer than 500 unique genes, or > 60% mitochondrial reads. Cloud-based Cumulus v1.0 was used to perform the bath correction (using the Harmony algorithm) on the aggregated gene-count matrices [82]. The number of cells after filtration in the current study was 3,263 in wild-type and 4,276 in *ctla-4*$^{-/-}$ groups, respectively. Cells were grouped into an optimal number of clusters for *de novo* cell type discovery using Seurat's FindNeighbors() and FindClusters() functions, graph-based clustering approach with visualization of cells being achieved through the use of t-SNE or UMAP plots [83]. The cell types were determined using a combination of marker genes identified from the literature and gene ontology. The marker genes were visualized by dot plot and t-SNE plots to reveal specific individual cell types.

16S rRNA sequencing analysis

Intestinal contents were collected from both wild-type and *ctla-4*$^{-/-}$ zebrafish by gently squeezing the intestines with fine-tipped tweezers, and the remaining intestines were used for single-cell RNA-sequencing analysis. Contents from six fish were pooled to form one replicate, with each experimental sample comprising four replicates. DNA was extracted from the samples using the CTAB method, a protocol known for its efficacy in isolating DNA from trace quantities. The quality of DNA was assessed

through agarose gel electrophoresis. Total DNA was amplified to construct sequencing libraries using primers (341F: 5'-CCTACGGGNGGCWGCAG-3'; 805R: 5'-GACTACHVGGGTATCTAATCC-3') targeting the V3-V4 regions of the 16S rRNA gene. The libraries were sequenced on an Illumina NovaSeq PE250 platform. Quality filtering was performed under specific conditions to obtain high-quality clean tags using fqtrim (v0.94). Chimeric sequences were removed using Vsearch software (v2.3.4). After dereplication using DADA2, a feature table and feature sequences were generated. Alpha diversity is applied in analyzing the complexity of species diversity for a sample through the Shannon and Simpson indices, with all calculations performed in QIIME2. Beta diversity analysis was also conducted in QIIME2, and the graphs were drawn by R package. Sequence alignment was performed using BLAST, and representative sequences were annotated using the SILVA database. Other diagrams were implemented using the R package (v3.5.2).

In vitro lymphocyte proliferation assay

The leukocytes were prepared from the spleen, kidney, and peripheral blood of wild-type (10 fish) or *ctla-4*$^{-/-}$ (10 fish) zebrafish through Ficoll-Hypaque centrifugation. A total of 2×10^6 leukocytes from either wild-type or *ctla-4*$^{-/-}$ individuals were labeled with 1 μM carboxyfluorescein succinimidyl ester (CFSE; Thermo Fisher Scientific) at 25℃ for 5 min. The reaction was terminated by adding a triploid volume of Leibovitz L-15 medium (Gibco) supplemented with 10% FBS, as previously described [84]. After washing with D-Hank's solution, the cells were cultured in L-15 medium containing 10% FBS in the presence or absence of PHA (5 μg/ml), recombinant Ctla-4-Ig (20 μg/ml),

Cd28-Ig (20 μg/ml), Cd80/86 (10 μg/ml) proteins or anti-Ctla-4 Ab (10 μg/ml) at 28℃ for 3 days. CFSE fluorescence intensity in the labeled co-cultures was analyzed using a flow cytometer (FACSJazz; BD Biosciences) to assess cell division [85].

Prediction of protein interactions by AlphaFold2

AlphaFold2 (version 2.3.2; available at https://github.com/google-deepmind/alphafold) was implemented on a high-performance computing cluster to predict the structures of the Cd80/86 complexes with Cd28 and Ctla-4 [85]. The resulting models were ranked based on their per-residue Local Distance Difference Test (pLDDT) scores, which quantify the confidence level of each residue on a scale from 0 to 100. Residues were color-coded according to their pLDDT scores, with higher values reflecting greater confidence in the prediction. Furthermore, the Predicted Aligned Error (PAE) scores were analyzed to identify well-defined interaction interfaces between Cd28 or Ctla-4 and Cd80/86.

Microscale thermophoresis assay

The binding affinity between Cd80/86 and Cd28/Ctla-4 were measured through microscale thermophoresis (MST) assays using a Monolith NT.115 instrument (Nano Temper Technologies) as previously described [86]. In each assay, the labeled proteins (Cd28/Ctla-4 with EGFP-tag) were incubated with varying concentrations of unlabeled ligand protein (Cd80/86) for 10 min at room temperature. The initial protein concentration of 3.2 μM was diluted into 16 different concentrations by doubling dilution. The samples were then loaded into capillaries and analyzed at 25℃ by using 40% light emitting diode (LED) and medium MST power. The binding affinities of

Cd80/86 with Cd28 and Cd80/86 with Ctla-4 were examined using the same parameters. Each assay was repeated three to five times, and dissociation constants (K_D) were calculated using MO.Affinity Analysis software.

In vivo administration of sCtla-4-Ig

An *in vivo* sCtla-4-Ig administration assay was conducted to evaluate the potential therapeutic effect of sCTLA-4-Ig on intervention of a *ctla-4*-deficiency induced IBD-like phenotype. For this procedure, the *ctla-4*$^{-/-}$ zebrafish were i.p administered with recombinant soluble Ctla-4-Ig protein (sCtla-4-Ig, 2 μg/g body weight) every other day until day 14. Fish that received an equal amount of human IgG isotype were used as control. The dose of sCtla-4-Ig was chosen based on its ability to significantly inhibit the mRNA expression of *il13* in Ctla-4-deficient zebrafish.

Statistical analysis

Statistical analysis and graphical presentation were performed with GraphPad Prism 8.0. All data were presented as the mean ± SD of each group. Statistical evaluation of differences was assessed using one-way ANOVA, followed by an unpaired two-tailed *t*-teat. Statistical significance was defined as $^{*}p < 0.05$, $^{**}p < 0.01$, $^{***}p < 0.001$, and $^{****}p < 0.0001$. All experiments were replicated at least three times.

Data availability

All data generated or analyzed during this study are included in this article and its supplementary information files. The RNA-seq and scRNA-seq data for this study have been deposited in NCBI Gene Expression Omnibus (GEO)

726 (https://www.ncbi.nlm.nih.gov/geo/) under accession numbers GSE255304 and
727 GSE255303, respectively. The 16S rRNA sequencing data in this study have been
728 deposited in the NCBI Sequence Read Archive (SRA)
729 (https://www.ncbi.nlm.nih.gov/sra/) with an accession number of BioProject
730 PRJNA1073727.
731

732 **Acknowledgements**

733 We are grateful to Bio-ultrastructure Analysis Laboratory at the Analysis Center
734 of Agrobiology and Environmental Sciences, Zhejiang University, for their assistance
735 in TEM sample preparation and observation. We also thank Hong Deng and Qiong
736 Huang for their valuable advice and expertise in pathological analysis. Additionally, we
737 acknowledge She-long Zhang for his support in two-photon laser confocal scanning
738 microscope capture. This work was supported by grants from the National Natural
739 Science Foundation of China (32173003) and the National Key Research and
740 Development Program of China (2018YFD0900503, 2018YFD0900505).
741

742 **Author Contributions**

743 L. L. Q. and J. Z. S. conceived and designed the experiments. L. L. Q. and C. B.
744 H. conducted the experiments. Data analysis was performed by L. L. Q., C. B. H., Q.
745 Z., Y. W., A. F. L., L. X. X., Y. C., and J. Z. S. Reagents, materials, and analysis tools
746 were contributed by L. X. X., D. D. F., and J. Z. S. The manuscript was written by L.
747 L. Q., Y. C., L. X. X., and J. Z. S. All authors reviewed the manuscript and provided

feedback.

Conflict of Interest

The authors declare that they have no competing financial interests.

Ethical approval and consent to participate

All animal experiments were performed with the approval of the Ethics Committee for Animal Experimentation of Zhejiang University.

REFERENCES

1. Hodson R (2016) Inflammatory bowel disease. Nature 540:S97-S97. https://10.1038/540S97a
2. Zhang Y Z, Li Y Y (2014) Inflammatory bowel disease: Pathogenesis. World J Gastroentero 20:91-99. https://10.3748/wjg.v20.i1.91
3. Venema W T C U, Voskuil M D, Dijkstra G, Weersma R K, Festen E A M (2017) The genetic background of inflammatory bowel disease: from correlation to causality. J Pathol 241:146-158. https://10.1002/path.4817
4. Loftus E V (2004) Clinical epidemiology of inflammatory bowel disease: Incidence, prevalence, and environmental influences. Gastroenterology 126:1504-1517. https://10.1053/j.gastro.2004.01.063
5. Khor B, Gardet A, Xavier R J (2011) Genetics and pathogenesis of inflammatory bowel disease. Nature 474:307-317. https://10.1038/nature10209
6. Neurath M F (2020) Host-microbiota interactions in inflammatory bowel disease. Nat Rev Gastro Hepat 17:76-77. https://10.1038/s41575-019-0248-1
7. Kordjazy N, Haj-Mirzaian A, Haj-Mirzaian A, Rohani M M, Gelfand E W, Rezaei N *et al.* (2018) Role of toll-like receptors in inflammatory bowel disease. Pharmacological Research 129:204-215. https://10.1016/j.phrs.2017.11.017
8. Horowitz J E, Warner N, Staples J, Crowley E, Gosalia N, Murchie R *et al.* (2021) Mutation spectrum of NOD2 reveals recessive inheritance as a main driver of Early Onset Crohn's Disease. Sci Rep-Uk 11:5595. https://10.1038/s41598-021-84938-8
9. Duerr R H, Taylor K D, Brant S R, Rioux J D, Silverberg M S, Daly M J *et al.* (2006) A genome-wide association study identifies IL23R as an inflammatory bowel disease gene. Science 314:1461-1463. https://10.1126/science.1135245
10. Tremelling M, Berzuini C, Massey D, Bredin F, Price C, Dawson C *et al.* (2008) Contribution

of TNFSF15 gene variants to Crohn's disease susceptibility confirmed in UK population. Inflamm Bowel Dis 14:733-737. https://10.1002/ibd.20399

11. Rudd C E, Schneider H (2003) Unifying concepts in CD28, ICOS and CTLA4 co-receptor signalling. Nat Rev Immunol 3:544-556. https://10.1038/nri1131

12. Yang Y, Li X, Ma Z, Wang C, Yang Q, Byrne-Steele M *et al.* (2021) CTLA-4 expression by B-1a B cells is essential for immune tolerance. Nat Commun 12:525. https://10.1038/s41467-020-20874-x

13. Kim G R, Choi J M (2022) Current Understanding of Cytotoxic T Lymphocyte Antigen-4 (CTLA-4) Signaling in T-Cell Biology and Disease Therapy. Mol Cells 45:513-521. https://10.14348/molcells.2022.2056

14. Marengere L E, Waterhouse P, Duncan G S, Mittrucker H W, Feng G S, Mak T W (1996) Regulation of T cell receptor signaling by tyrosine phosphatase SYP association with CTLA-4. Science 272:1170-1173. https://10.1126/science.272.5265.1170

15. Lee K M, Chuang E, Griffin M, Khattri R, Hong D K, Zhang W G *et al.* (1998) Molecular basis of T cell inactivation by CTLA-4. Science 282:2263-2266. https://10.1126/science.282.5397.2263

16. Yokosuka T, Kobayashi W, Takamatsu M, Sakata-Sogawa K, Zeng H, Hashimoto-Tane A *et al.* (2010) Spatiotemporal Basis of CTLA-4 Costimulatory Molecule-Mediated Negative Regulation of T Cell Activation. Immunity 33:326-339. https://10.1016/j.immuni.2010.09.006

17. Linsley P S, Greene J L, Brady W, Bajorath J, Ledbetter J A, Peach R (1994) Human B7-1 (Cd80) and B7-2 (Cd86) Bind with Similar Avidities but Distinct Kinetics to Cd28 and Ctla-4 Receptors. Immunity 1:793-801. https://10.1016/S1074-7613(94)80021-9

18. Collins A V, Brodie D W, Gilbert R J, Iaboni A, Manso-Sancho R, Walse B *et al.* (2002) The interaction properties of costimulatory molecules revisited. Immunity 17:201-210. https://10.1016/s1074-7613(02)00362-x

19. Saito T, Yokosuka T, Hashimoto-Tane A (2010) Dynamic regulation of T cell activation and co-stimulation through TCR-microclusters. Febs Lett 584:4865-4871. https://10.1016/j.febslet.2010.11.036

20. Tivol E A, Borriello F, Schweitzer A N, Lynch W P, Bluestone J A, Sharpe A H (1995) Loss of Ctla-4 Leads to Massive Lymphoproliferation and Fatal Multiorgan Tissue Destruction, Revealing a Critical Negative Regulatory Role of Ctla-4. Immunity 3:541-547. https://10.1016/1074-7613(95)90125-6

21. Waterhouse P, Penninger J M, Timms E, Wakeham A, Shahinian A, Lee K P *et al.* (1995) Lymphoproliferative Disorders with Early Lethality in Mice Deficient in Ctla-4. Science 270:985-988. https://10.1126/science.270.5238.985

22. Chambers C A, Sullivan T J, Allison J P (1997) Lymphoproliferation in CTLA-4-deficient mice is mediated by costimulation-dependent activation of CD4(+) T cells. Immunity 7:885-895. https://10.1016/S1074-7613(00)80406-9

23. Khattri R, Auger J A, Griffin M D, Sharpe A H, Bluestone J A (1999) Lymphoproliferative Disorder in CTLA-4 Knockout Mice Is Characterized by CD28-Regulated Activation of Th2 Responses. The Journal of Immunology 162:5784-5791. https://10.4049/jimmunol.162.10.5784

24. Bour-Jordan H, Grogan J L, Tang Q Z, Auger J A, Locksley R M, Bluestone J A (2003) CTLA-

4 regulates the requirement for cytokine-induced signals in T_H2 lineage commitment. Nature Immunology 4:182-188. https://10.1038/ni884

25. Klocke K, Sakaguchi S, Holmdahl R, Wing K (2016) Induction of autoimmune disease by deletion of CTLA-4 in mice in adulthood. Proc Natl Acad Sci U S A 113:E2383-2392. https://10.1073/pnas.1603892113

26. Wing K, Onishi Y, Prieto-Martin P, Yamaguchi T, Miyara M, Fehervari Z *et al.* (2008) CTLA-4 control over Foxp3+ regulatory T cell function. Science 322:271-275. https://10.1126/science.1160062

27. Repnik K, Potocnik U (2010) CT60 Single-Nucleotide Polymorphism Is Associated with Slovenian Inflammatory Bowel Disease Patients and Regulates Expression of Isoforms. DNA Cell Biol 29:603-610. https://10.1089/dna.2010.1021

28. Xia B, Crusius J B A, Wu J, Zwiers A, van Bodegraven A A, Peña A S (2002) CTLA-4 gene polymorphisms in Dutch and Chinese patients with inflammatory bowel disease. Scand J Gastroentero 37:1296-1300. https://10.1080/003655202761020579

29. Jiang T, Ge L Q, Chen Z T, Li C, Zhou F, Luo Y *et al.* (2010) Effect of cytotoxic T lymphocyte-associated molecule 4 1661 gene polymorphism on its expression and transcription in ulcerative colitis. J Digest Dis 11:369-375. https://10.1111/j.1751-2980.2010.00462.x

30. Bamias G, Delladetsima I, Perdiki M, Siakavellas S I, Goukos D, Papatheodoridis G V *et al.* (2017) Immunological Characteristics of Colitis Associated with Anti-CTLA-4 Antibody Therapy. Cancer Invest 35:443-455. https://10.1080/07357907.2017.1324032

31. Lo B C, Kryczek I, Yu J, Vatan L, Caruso R, Matsumoto M *et al.* (2024) Microbiota-dependent activation of CD4+ T cells induces CTLA-4 blockade–associated colitis via Fcγ receptors. Science 383:62-70. https://10.1126/science.adh8342

32. Cooper M D, Alder M N (2006) The evolution of adaptive immune systems. Cell 124:815-822. https://10.1016/j.cell.2006.02.001

33. Lam S H, Chua H L, Gong Z, Lam T J, Sin Y M (2004) Development and maturation of the immune system in zebrafish, Danio rerio: a gene expression profiling, in situ hybridization and immunological study. Dev Comp Immunol 28:9-28. https://10.1016/s0145-305x(03)00103-4

34. Peach R J, Bajorath J, Brady W, Leytze G, Greene J, Naemura J *et al.* (1994) Complementarity-Determining Region-1 (Cdr1)-Analogous and Cdr3-Analogous Regions in Ctla-4 and Cd28 Determine the Binding to B7-1. J Exp Med 180:2049-2058. https://10.1084/jem.180.6.2049

35. Shiratori T, Miyatake S, Ohno H, Nakaseko C, Isono K, Bonifacino J S *et al.* (1997) Tyrosine phosphorylation controls internalization of CTLA-4 by regulating its interaction with clathrin-associated adaptor complex AP-2. Immunity 6:583-589. https://10.1016/s1074-7613(00)80346-5

36. Bernard D, Riteau B, Hansen J D, Phillips R B, Michel F, Boudinot P *et al.* (2006) Costimulatory receptors in a teleost fish: Typical CD28, elusive CTLA4. Journal of Immunology 176:4191-4200. https://10.4049/jimmunol.176.7.4191

37. Hu C B, Wang J, Hong Y, Li H, Fan D D, Lin A F *et al.* (2023) Single-cell transcriptome profiling reveals diverse immune cell populations and their responses to viral infection in the spleen of zebrafish. Faseb J 37:e22951. https://10.1096/fj.202201505RRRR

38. Butin-Israeli V, Bui T M, Wiesolek H L, Mascarenhas L, Lee J J, Mehl L C *et al.* (2019)

Neutrophil-induced genomic instability impedes resolution of inflammation and wound healing. J Clin Invest 129:712-726. https://10.1172/JCI122085

39. Lees C W, Barrett J C, Parkes M, Satsangi J (2011) New IBD genetics: common pathways with other diseases. Gut 60:1739-1753. https://10.1136/gut.2009.199679

40. Lee J C, Biasci D, Roberts R, Gearry R B, Mansfield J C, Ahmad T *et al.* (2017) Genome-wide association study identifies distinct genetic contributions to prognosis and susceptibility in Crohn's disease. Nat Genet 49:262-268. https://10.1038/ng.3755

41. Bernink J H, Peters C P, Munneke M, te Velde A A, Meijer S L, Weijer K *et al.* (2013) Human type 1 innate lymphoid cells accumulate in inflamed mucosal tissues. Nat Immunol 14:221-229. https://10.1038/ni.2534

42. Li J, Doty A L, Tang Y, Berrie D, Iqbal A, Tan S A *et al.* (2017) Enrichment of IL-17A(+) IFN-gamma(+) and IL-22(+) IFN-gamma(+) T cell subsets is associated with reduction of NKp44(+) ILC3s in the terminal ileum of Crohn's disease patients. Clin Exp Immunol 190:143-153. https://10.1111/cei.12996

43. Martin J C, Chang C, Boschetti G, Ungaro R, Giri M, Grout J A *et al.* (2019) Single-Cell Analysis of Crohn's Disease Lesions Identifies a Pathogenic Cellular Module Associated with Resistance to Anti-TNF Therapy. Cell 178:1493-1508 e1420. https://10.1016/j.cell.2019.08.008

44. Buonocore S, Ahern P P, Uhlig H H, Ivanov, II, Littman D R, Maloy K J *et al.* (2010) Innate lymphoid cells drive interleukin-23-dependent innate intestinal pathology. Nature 464:1371-1375. https://10.1038/nature08949

45. Ermann J, Staton T, Glickman J N, de Waal Malefyt R, Glimcher L H (2014) Nod/Ripk2 signaling in dendritic cells activates IL-17A-secreting innate lymphoid cells and drives colitis in T-bet-/-.Rag2-/- (TRUC) mice. Proc Natl Acad Sci U S A 111:E2559-2566. https://10.1073/pnas.1408540111

46. Aparicio-Domingo P, Romera-Hernandez M, Karrich J J, Cornelissen F, Papazian N, Lindenbergh-Kortleve D J *et al.* (2015) Type 3 innate lymphoid cells maintain intestinal epithelial stem cells after tissue damage. J Exp Med 212:1783-1791. https://10.1084/jem.20150318

47. Ott S J, Musfeldt M, Wenderoth D F, Hampe J, Brant O, Folsch U R *et al.* (2004) Reduction in diversity of the colonic mucosa associated bacterial microflora in patients with active inflammatory bowel disease. Gut 53:685-693. https://10.1136/gut.2003.025403

48. Manichanh C, Rigottier-Gois L, Bonnaud E, Gloux K, Pelletier E, Frangeul L *et al.* (2006) Reduced diversity of faecal microbiota in Crohn's disease revealed by a metagenomic approach. Gut 55:205-211. https://10.1136/gut.2005.073817

49. Zhao Q, Chang H, Zheng J, Li P, Ye L, Pan R *et al.* (2023) A novel Trmt5-deficient zebrafish model with spontaneous inflammatory bowel disease-like phenotype. Signal Transduct Target Ther 8:86. https://10.1038/s41392-023-01318-6

50. Xu Z, Takizawa F, Casadei E, Shibasaki Y, Ding Y, Sauters T J C *et al.* (2020) Specialization of mucosal immunoglobulins in pathogen control and microbiota homeostasis occurred early in vertebrate evolution. Sci Immunol 5:3254-3271. https://10.1126/sciimmunol.aay3254

51. Belzer C, de Vos W M (2012) Microbes inside--from diversity to function: the case of Akkermansia. ISME J 6:1449-1458. https://10.1038/ismej.2012.6

914 52. Hosseini A, Gharibi T, Marofi F, Babaloo Z, Baradaran B (2020) CTLA-4: From mechanism
915 to autoimmune therapy. Int Immunopharmacol 80:106221.
916 https://10.1016/j.intimp.2020.106221
917 53. Sun W H, Zhang X M, Wu J, Zhao W D, Zhao S X, Li M L (2019) Correlation of TSHR and
918 CTLA-4 Single Nucleotide Polymorphisms with Graves Disease. Int J Genomics
919 2019:6982623. https://10.1155/2019/6982623
920 54. Vergara A, De Felice M, Cesaro A, Gragnano F, Pariggiano I, Golia E *et al.* (2023) Immune-
921 Checkpoint Inhibitor-Related Myocarditis: Where We Are and Where We Will Go.
922 Angiology 12:33197231201929. https://10.1177/00033197231201929
923 55. Kheiralla K E K (2021) CTLA-4 (+49A/G) Polymorphism in Type 1 Diabetes Children of
924 Sudanese Population. Glob Med Genet 8:11-18. https://10.1055/s-0041-1723008
925 56. Lin T W, Hu Y C, Yang Y H, Chien Y H, Lee N C, Yu H H *et al.* (2022) CTLA-4 gene mutation
926 and multiple sclerosis: A case report and literature review. J Microbiol Immunol 55:545-
927 548. https://10.1016/j.jmii.2021.10.009
928 57. Cutolo M, Sulli A, Paolino S, Pizzorni C (2016) CTLA-4 blockade in the treatment of
929 rheumatoid arthritis: an update. Expert Rev Clin Immu 12:417-425.
930 https://10.1586/1744666x.2016.1133295
931 58. Chang M C, Chang Y T, Tien Y W, Liang P C, Jan I S, Wei S C *et al.* (2007) T-Cell regulatory
932 gene CTLA-4 Polymorphism/Haplotype association with autoimmune pancreatitis. Clin
933 Chem 53:1700-1705. https://10.1373/clinchem.2007.085951
934 59. Fathima N, Narne P, Ishaq M (2019) Association and gene-gene interaction analyses for
935 polymorphic variants in CTLA-4 and FOXP3 genes: role in susceptibility to autoimmune
936 thyroid disease. Endocrine 64:591-604. https://10.1007/s12020-019-01859-3
937 60. Zeissig S, Petersen B S, Tomczak M, Melum E, Huc-Claustre E, Dougan S K *et al.* (2015)
938 Early-onset Crohn's disease and autoimmunity associated with a variant in CTLA-4. Gut
939 64:1889-1897. https://10.1136/gutjnl-2014-308541
940 61. Angelino G, Cifaldi C, Zangari P, Di Cesare S, Di Matteo G, Chiriaco M *et al.* (2021) Gastric
941 cancer, inflammatory bowel disease and polyautoimmunity in a 17-year-old boy: CTLA-
942 4 deficiency successfully treated with Abatacept. Eur J Gastroen Hepat 33:E1051-E1056.
943 https://10.1097/Meg.0000000000002185
944 62. Liu J Z, van Sommeren S, Huang H L, Ng S C, Alberts R, Takahashi A *et al.* (2015)
945 Association analyses identify 38 susceptibility loci for inflammatory bowel disease and
946 highlight shared genetic risk across populations. Nat Genet 47:979-+.
947 https://10.1038/ng.3359
948 63. Kim J J, Shajib M S, Manocha M M, Khan W I (2012) Investigating Intestinal Inflammation
949 in DSS-induced Model of IBD. Jove-J Vis Exp 10.3791/3678https://10.3791/3678
950 64. Geiger B, Zhen A W, Kokkotou E, Fraenkel P G (2013) Granulocytes Infiltrate The Intestine
951 In a Zebrafish Model Of Inflammatory Bowel Disease. Blood
952 122:https://10.1182/blood.V122.21.2276.2276
953 65. Fleming A, Jankowski J, Goldsmith P (2010) In Vivo Analysis of Gut Function and Disease
954 Changes in a Zebrafish Larvae Model of Inflammatory Bowel Disease: A Feasibility Study.
955 Inflamm Bowel Dis 16:1162-1172. https://10.1002/ibd.21200
956 66. Oehlers S H, Flores M V, Hall C J, Crosier K E, Crosier P S (2012) Retinoic acid suppresses
957 intestinal mucus production and exacerbates experimental enterocolitis. Dis Model Mech

5:457-467. https://10.1242/dmm.009365

67. Coronado M, Solis C J, Hernandez P P, Feijóo C G (2019) Soybean Meal-Induced Intestinal Inflammation in Zebrafish Is T Cell-Dependent and Has a Th17 Cytokine Profile. Frontiers in Immunology 10:610-622. https://10.3389/fimmu.2019.00610

68. Al-Sadi R, Guo S H, Ye D M, Dokladny K, Alhmoud T, Ereifej L *et al.* (2013) Mechanism of IL-1b Modulation of Intestinal Epithelial Barrier Involves p38 Kinase and Activating Transcription Factor-2 Activation. Journal of Immunology 190:6596-6606. https://10.4049/jimmunol.1201876

69. Al-Sadi R, Guo S H, Ye D M, Ma T Y (2013) TNF-α Modulation of Intestinal Epithelial Tight Junction Barrier Is Regulated by ERK1/2 Activation of Elk-1. Am J Pathol 183:1871-1884. https://10.1016/j.ajpath.2013.09.001

70. Heller F, Florian P, Bojarski C, Richter J, Christ M, Hillenbrand B *et al.* (2005) Interleukin-13 is the key effector Th2 cytokine in ulcerative colitis that affects epithelial tight junctions, apoptosis, and cell restitution. Gastroenterology 129:550-564. https://10.1016/j.gastro.2005.05.002

71. Shin N R, Whon T W, Bae J W (2015) Proteobacteria: microbial signature of dysbiosis in gut microbiota. Trends Biotechnol 33:496-503. https://10.1016/j.tibtech.2015.06.011

72. Winter S E, Lopez C A, Bäumler A J (2013) The dynamics of gut-associated microbial communities during inflammation. Embo Rep 14:319-327. https://10.1038/embor.2013.27

73. Ott S J, Musfeldt M, Wenderoth D F, Hampe J, Brant O, Fölsch U R *et al.* (2004) Reduction in diversity of the colonic mucosa associated bacterial microflora in patients with active inflammatory bowel disease. Gut 53:685-693. https://10.1136/gut.2003.025403

74. Hughes E R, Winter M G, Duerkop B A, Spiga L, de Carvalho T F, Zhu W H *et al.* (2017) Microbial Respiration and Formate Oxidation as Metabolic Signatures of Inflammation-Associated Dysbiosis. Cell Host Microbe 21:208-219. https://10.1016/j.chom.2017.01.005

75. Ahmed A, Joseph A M, Zhou J, Horn V, Uddin J, Lyu M *et al.* (2024) CTLA-4-expressing ILC3s restrain interleukin-23-mediated inflammation. Nature 630:976-983. https://10.1038/s41586-024-07537-3

76. Shi W, Shao T, Li J Y, Fan D D, Lin A F, Xiang L X *et al.* (2019) BTLA-HVEM Checkpoint Axis Regulates Hepatic Homeostasis and Inflammation in a ConA-Induced Hepatitis Model in Zebrafish. Journal of Immunology 203:2425-2442. https://10.4049/jimmunol.1900458

77. Linsley P S, Brady W, Grosmaire L, Aruffo A, Damle N K, Ledbetter J A (1991) Binding of the B cell activation antigen B7 to CD28 costimulates T cell proliferation and interleukin 2 mRNA accumulation. J Exp Med 173:721-730. https://10.1084/jem.173.3.721

78. Shi W, Shao T, Li J Y, Fan D D, Lin A F, Xiang L X *et al.* (2019) BTLA-HVEM Checkpoint Axis Regulates Hepatic Homeostasis and Inflammation in a ConA-Induced Hepatitis Model in Zebrafish. J Immunol 203:2425-2442. https://10.4049/jimmunol.1900458

79. Erben U, Loddenkemper C, Doerfel K, Spieckermann S, Haller D, Heimesaat M M *et al.* (2014) A guide to histomorphological evaluation of intestinal inflammation in mouse models. Int J Clin Exp Pathol 7:4557-4576.

80. Kohl M, Wiese S, Warscheid B (2011) Cytoscape: software for visualization and analysis of biological networks. Methods Mol Biol 696:291-303. https://10.1007/978-1-60761-987-1_18

81. McGinnis C S, Murrow L M, Gartner Z J (2019) DoubletFinder: Doublet Detection in Single-Cell RNA Sequencing Data Using Artificial Nearest Neighbors. Cell Syst 8:329-+. https://10.1016/j.cels.2019.03.003

82. Li B, Gould J, Yang Y, Sarkizova S, Tabaka M, Ashenberg O *et al.* (2020) Cumulus provides cloud-based data analysis for large-scale single-cell and single-nucleus RNA-seq. Nat Methods 17:793-798. https://10.1038/s41592-020-0905-x

83. Cronan M R, Hughes E J, Brewer W J, Viswanathan G, Hunt E G, Singh B *et al.* (2021) A non-canonical type 2 immune response coordinates tuberculous granuloma formation and epithelialization. Cell 184:1757-1774 e1714. https://10.1016/j.cell.2021.02.046

84. Quah B J C, Warren H S, Parish C R (2007) Monitoring lymphocyte proliferation and with the intracellular fluorescent dye carboxyfluorescein diacetate succinimidyl ester. Nature Protocols 2:2049-2056. https://10.1038/nprot.2007.296

85. Rieder S A, Wang J Y, White N, Qadri A, Menard C, Stephens G *et al.* (2021) B7-H7 (HHLA2) inhibits T-cell activation and proliferation in the presence of TCR and CD28 signaling. Cell Mol Immunol 18:1503-1511. https://10.1038/s41423-020-0361-7

86. Jerabek-Willemsen M, André T, Wanner R, Roth H M, Duhr S, Baaske P *et al.* (2014) MicroScale Thermophoresis: Interaction analysis and beyond. J Mol Struct 1077:101-113. https://10.1016/j.molstruc.2014.03.009

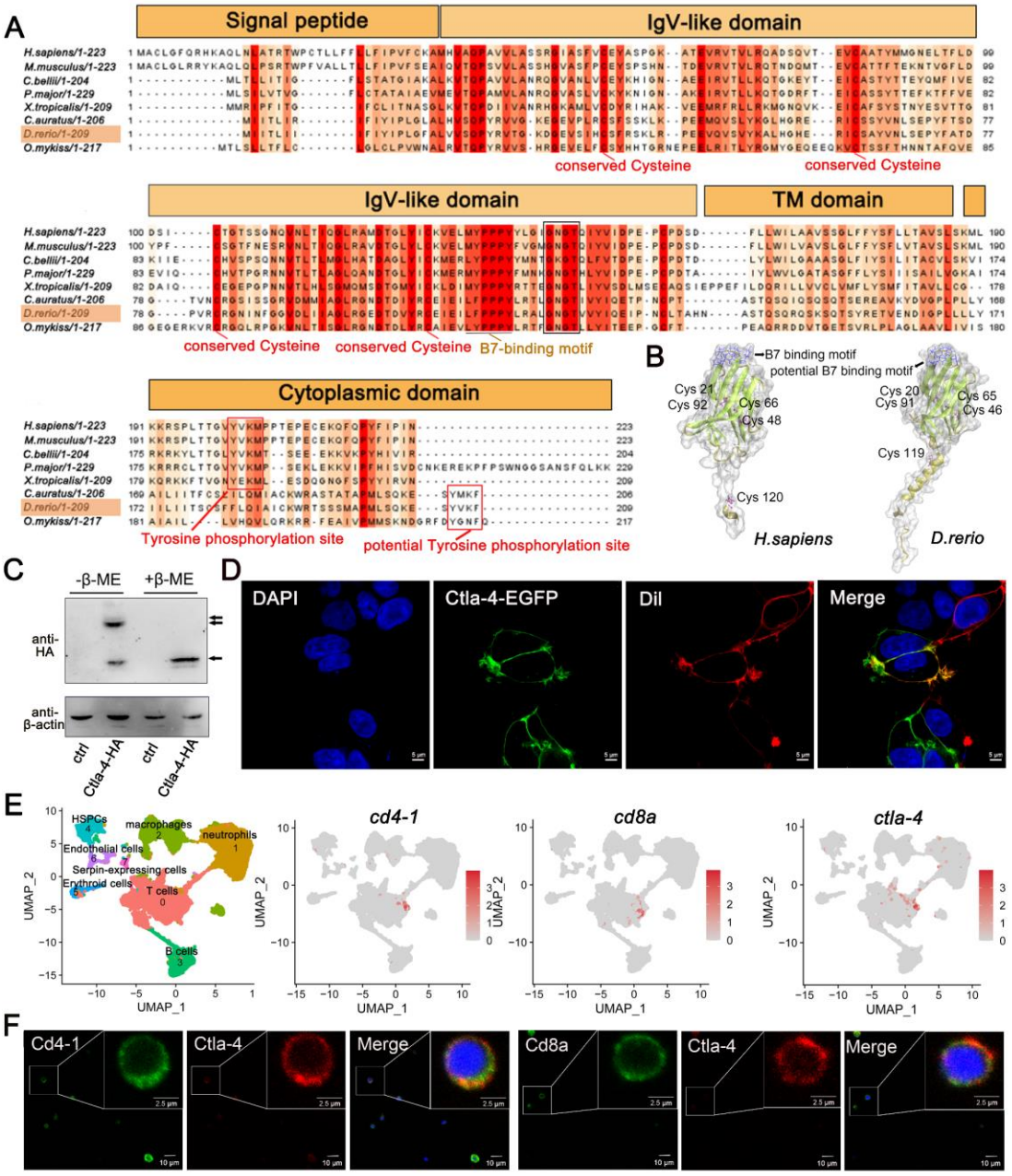

Fig.1 Characterization of zebrafish Ctla-4. **A** Alignment of the Ctla-4 homologs from different species generated with ClustalX and Jalview. The conserved and partially conserved amino acid residues in each species are colored in hues graded from orange to red, respectively. Key features, including conserved cysteine residues, functional motifs, such as B7-binding motif, tyrosine phosphorylation site, and potential tyrosine phosphorylation site, were indicated separately. The signal peptide, IgV-like domain, transmembrane (TM) domain, and cytoplasmic domain were marked above the

sequence. **B** The tertiary structure of the zebrafish Ctla-4 ectodomain, as predicted by AlphaFold2, was compared with that of humans. The two pairs of disulfide bonds (Cys^{20}-Cys^{91}/Cys^{46}-Cys^{65} in zebrafish and Cys^{21}-Cys^{92}/Cys^{48}-Cys^{66} in humans) used to connect the two-layer β-sandwich, and the separate Cys residue (Cys^{119} in zebrafish and Cys^{120} in humans) involved in the dimerization of the proteins are indicated. Cysteine residues are represented in purple ball-and-stick models, and the identified or potential B7 binding sites are highlighted in blue. **C** Dimer of Ctla-4 was identified by Western blot under reducing (+β-ME) or non-reducing (-β-ME) conditions. The ctrl represents a control sample derived from cells transfected with an empty plasmid. The monomers and dimers were indicated by single and double arrows, respectively. **D** The subcellular localization of Ctla-4 protein was assessed in HEK293T cells transfected with pEGFPN1-Ctla-4 for 48 hours, imaged using a two-photon laser-scanning microscope (Original magnification, 630×). Nuclei were stained with DAPI (blue), and cell membranes were stained with DiI (red). **E** UMAP plots showing the relative distribution of common T cell markers (*cd4-1*, *cd8a* and *ctla-4*) based on a splenic single-cell RNA sequencing (scRNA-seq) dataset we recently established [37]. **F** Immunofluorescence staining of lymphocytes isolated from zebrafish blood, spleen, and kidney. Cells were stained with mouse anti-Ctla-4, together with rabbit anti-Cd4-1 or rabbit anti-Cd8α. DAPI stain shows the location of the nuclei. Images were obtained using a two-photon laser-scanning microscope (Original magnification, 630×).

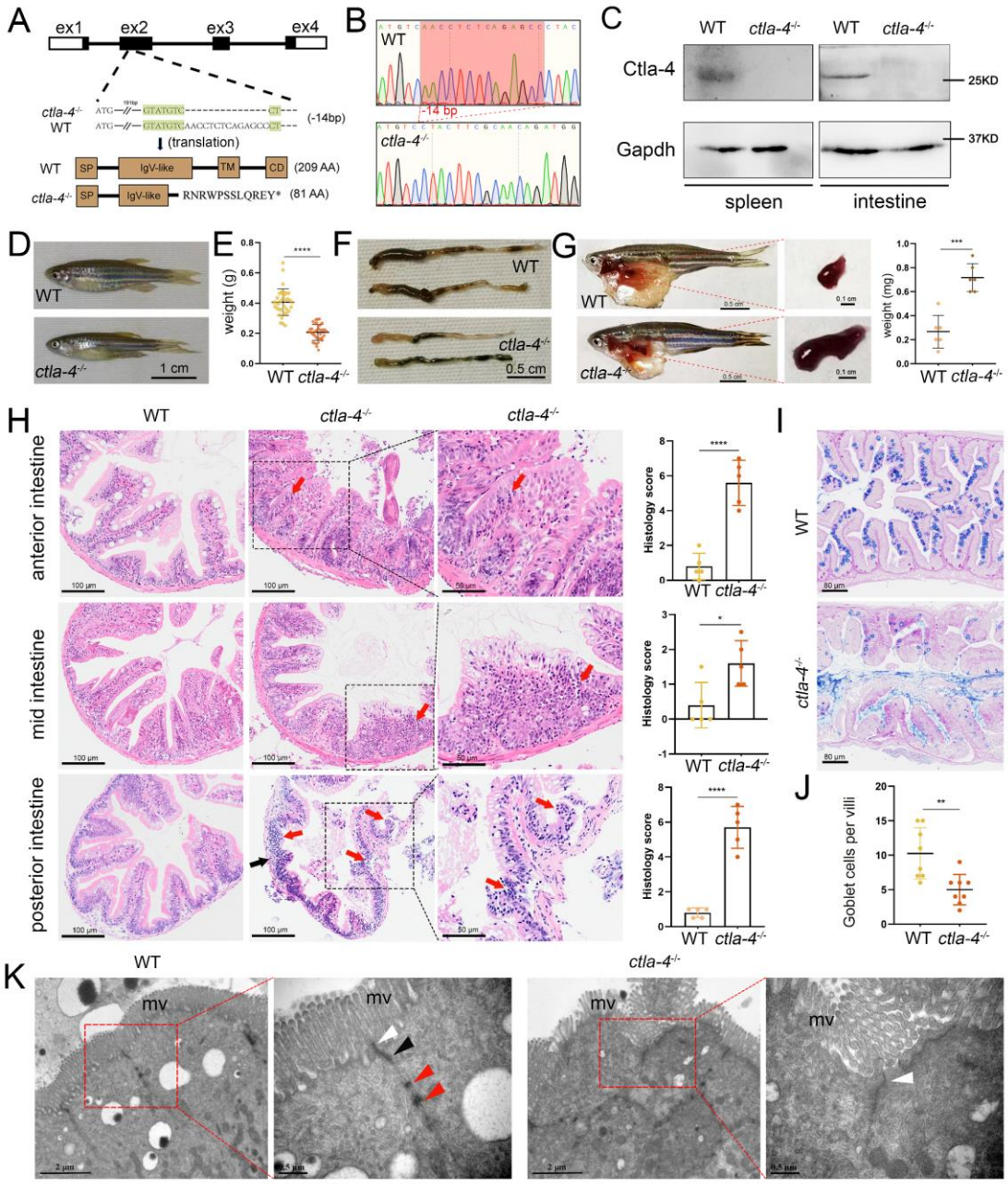

Fig.2 Examination on the IBD-like phenotype in *ctla-4*$^{-/-}$ zebrafish. **A** Generation of a homozygous *ctla-4*-deficient (*ctla-4*$^{-/-}$) zebrafish line through CRISPR/Cas9-based knockout of *ctla-4* gene on chromosome 9. A 14-bp deletion mutation in exon 2 results in a premature stop at codon 82, which is predicted to produce a defective Ctla-4 protein containing 81 amino acids. **B** Genotyping of the deficiency of *ctla-4* gene by Sanger sequencing. **C** Knockout efficiency of Ctla-4 selectively examined in spleen and gut

tissues of *ctla-4*$^{-/-}$ zebrafish by Western blot analysis. Gapdh serves as a loading control. **D** Normal gross appearance of adult wild-type (WT) and *ctla-4*$^{-/-}$ zebrafish. **E** Body weight statistics of WT and *ctla-4*$^{-/-}$ zebrafish (n = 30). **F** The change of intestine length in WT and *ctla-4*$^{-/-}$ zebrafish. **G** The change of splenic size in WT and *ctla-4*$^{-/-}$ zebrafish. **H** Representative H&E staining analysis of histopathological changes and quantitation of histology scores in the anterior, mid and posterior intestines from WT and *ctla-4*$^{-/-}$ zebrafish. Red arrows denote mucosal inflammatory cell infiltration, and black arrow indicates transmural inflammatory cell infiltration. **I** AB-PAS staining was used to analyze the mucin components and the number of goblet cells in anterior intestine from WT and *ctla-4*$^{-/-}$ zebrafish (n = 5). **J** Quantitation analysis of goblet cells of each villus in the foregut of WT and *ctla-4*$^{-/-}$ zebrafish (n = 8). **K** Observation of cell junctions between intestinal epithelial cells in posterior intestines from WT and *ctla-4*$^{-/-}$ zebrafish under TEM (Hitachi Model H-7650). White triangles indicate tight junctions, black triangle indicates adhesion junctions, and red triangles indicate desmosomes. Data are presented as mean ± standard deviation (SD). Statistical significance was assessed through an unpaired Student's t test ($^{*}p < 0.05$; $^{**}p < 0.01$; $^{***}p < 0.001$; $^{****}p < 0.0001$).

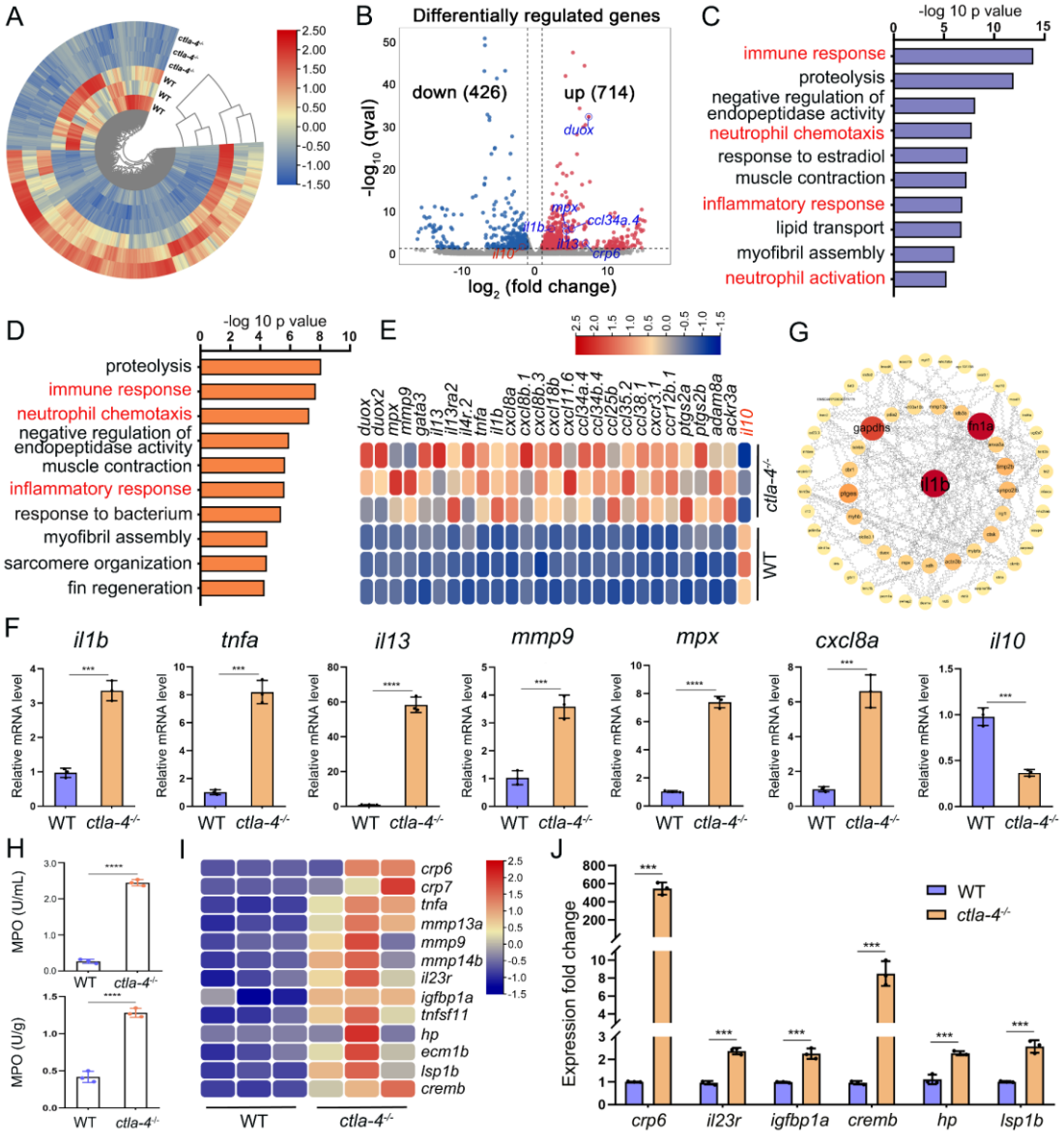

Fig.3 RNA-sequencing analysis of the molecular implications associated with the IBD-like phenotype in *ctla-4*$^{-/-}$ zebrafish. **A** Heatmap of different expressed genes between the intestines from wild-type (WT) and *ctla-4*$^{-/-}$ zebrafish. **B** Volcano plot showing the up-/down-regulated genes in the intestines of *ctla-4*$^{-/-}$ zebrafish compared with those of WT zebrafish. Red represents up-regulated genes, while blue denotes down-regulated genes. **C** GO analysis showing top 10 terms in biological processes of DEGs. **D** GO analysis showing top 10 terms in biological processes of all up-regulated genes. **E** Heatmap showing row-scaled expression of the representative differently expressed

inflammation and chemotaxis-related genes. **F** The mRNA expression levels of important genes associated with inflammation and chemokines confirmed by real-time qPCR. **G** Protein-protein interaction network was constructed using the DEGs. The nodes represent the proteins (genes); the edges represent the interaction of proteins (genes). **H** The MPO activity in the intestines (up) and peripheral blood (down). **I** Heatmap showing row-scaled expression of the IBD biomarker genes and IBD-related genes. **J** The mRNA expression levels of representative IBD biomarker genes and IBD-related genes were analyzed by real-time qPCR. Data are presented as mean ± standard deviation (SD). Statistical significance was assessed through an unpaired Student's t test ($^{**}p < 0.01$; $^{***}p < 0.001$; $^{****}p < 0.0001$).

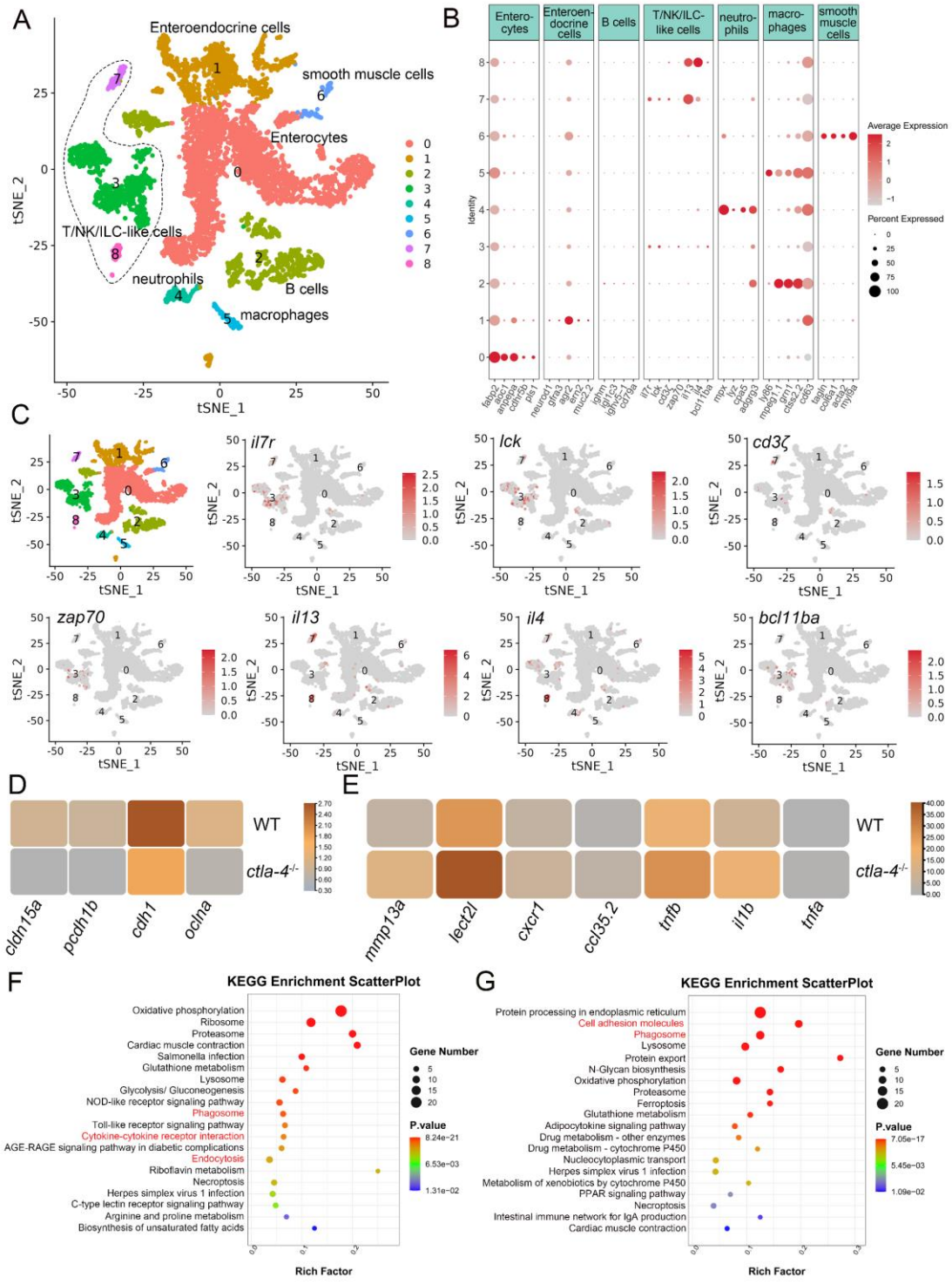

Fig.4 Single-cell RNA sequencing analysis of the major cell types associated with the IBD-like phenotype in *ctla-4*$^{-/-}$ zebrafish. **A** Classification of cell types from zebrafish intestines by tSNE embedding. **B** Dot plot showing the expression levels of lineage marker genes and percentage of cells per cluster that express the gene of interest. **C**

Expression maps of T cell associated markers within the cell populations of the zebrafish intestines. **D** Heatmap showing the mean expression levels of genes associated with tight and adhesion junctions in enterocytes across samples from wild-type (WT) and *ctla-4*$^{-/-}$ zebrafish. **E** Heatmap showing the mean expression levels of inflammation-related genes involved in cytokine-cytokine receptor interactions in neutrophils from WT and *ctla-4*$^{-/-}$ zebrafish samples. **F** KEGG enrichment analysis showing the top 15 terms of up-regulated genes in neutrophils from the *ctla-4*$^{-/-}$ sample versus the WT sample. **G** KEGG enrichment analysis showing the top 15 terms of up-regulated genes in macrophages from the *ctla-4*$^{-/-}$ sample versus the WT sample.

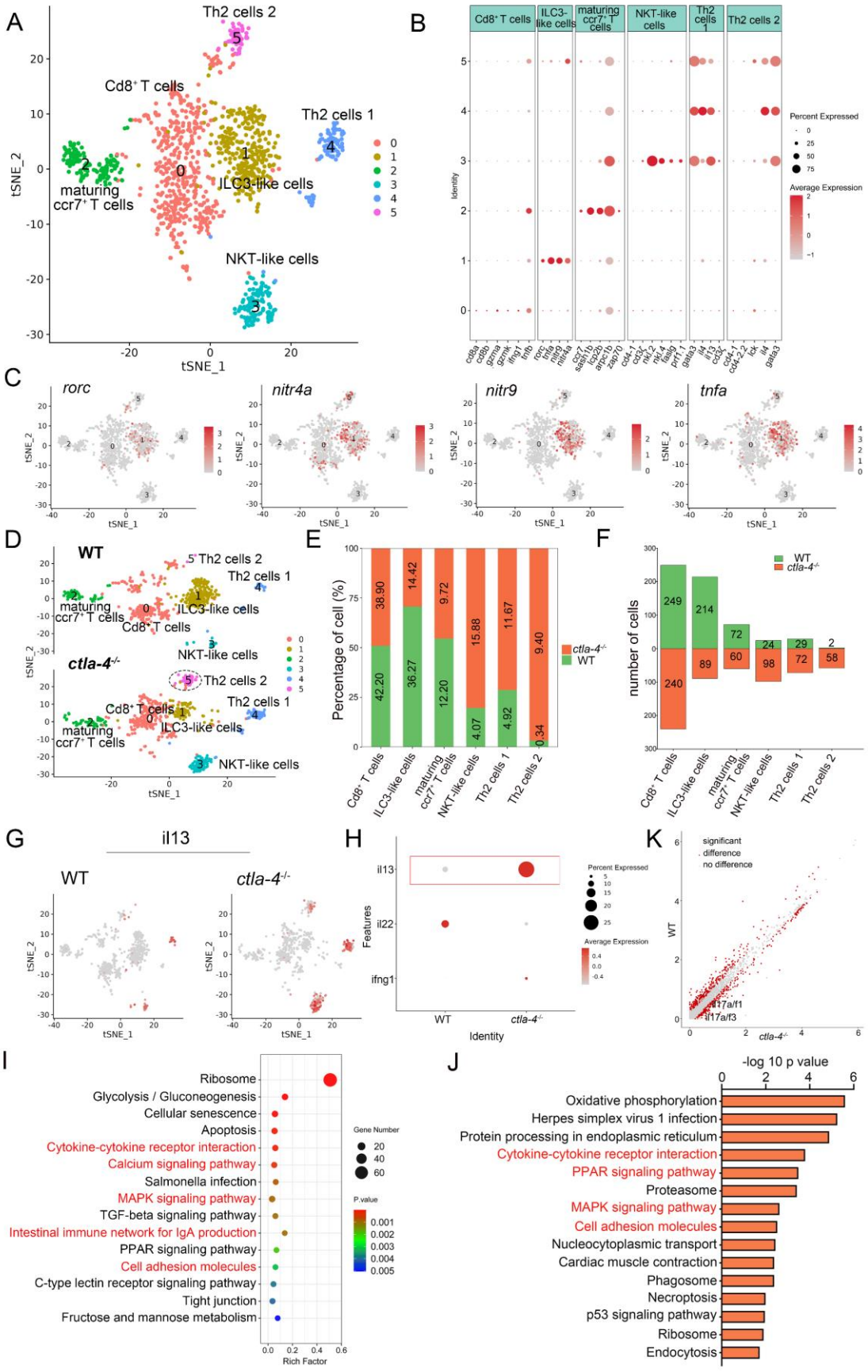

Fig.5 Single-cell RNA sequencing analysis of the subset immune-cells associated with

the IBD-like phenotype in *ctla-4*$^{-/-}$ zebrafish. **A** Classification of subset cells from the T/NK/ILC-like group by tSNE embedding. **B** Dot plot showing the mean expression levels of subset marker genes and percentage of cells per cluster that express the gene of interest. **C** Marker gene expression in individual cluster identifying this cluster as ILC3-like cells. **D** Changes in the composition of subset cells between samples from wild-type (WT) and *ctla-4*$^{-/-}$ zebrafish. A significantly increased Th2 subset (referred to as Th2 cells 2) in the *ctla-4*$^{-/-}$ sample was highlighted with a black dashed circle. **E** Histogram showing the different ratios of subset cells between the WT and *ctla-4*$^{-/-}$ samples. **F** Histogram presenting the different numbers of subset cells between the WT and *ctla-4*$^{-/-}$ samples. **G** Mean expression levels of the cytokine *il13* within different subset cells between the WT and *ctla-4*$^{-/-}$ samples. **H** Dot plot illustrating the mean expression of *il13* in T/NK/ILC-like cells from WT and *ctla-4*$^{-/-}$ zebrafish. **I** KEGG enrichment analysis showing the top 15 terms of the Th2 cells 2 genes from *ctla-4*$^{-/-}$ zebrafish. **J** KEGG enrichment analysis showing the top 15 terms of up-regulated genes in NKT-like cells. **K** Scatter plot showing the DEGs of ILC3-like cells in WT and *ctla-4*$^{-/-}$ zebrafish. The *il17a/f1* and *il17a/f3* was shown in the scatter plot.

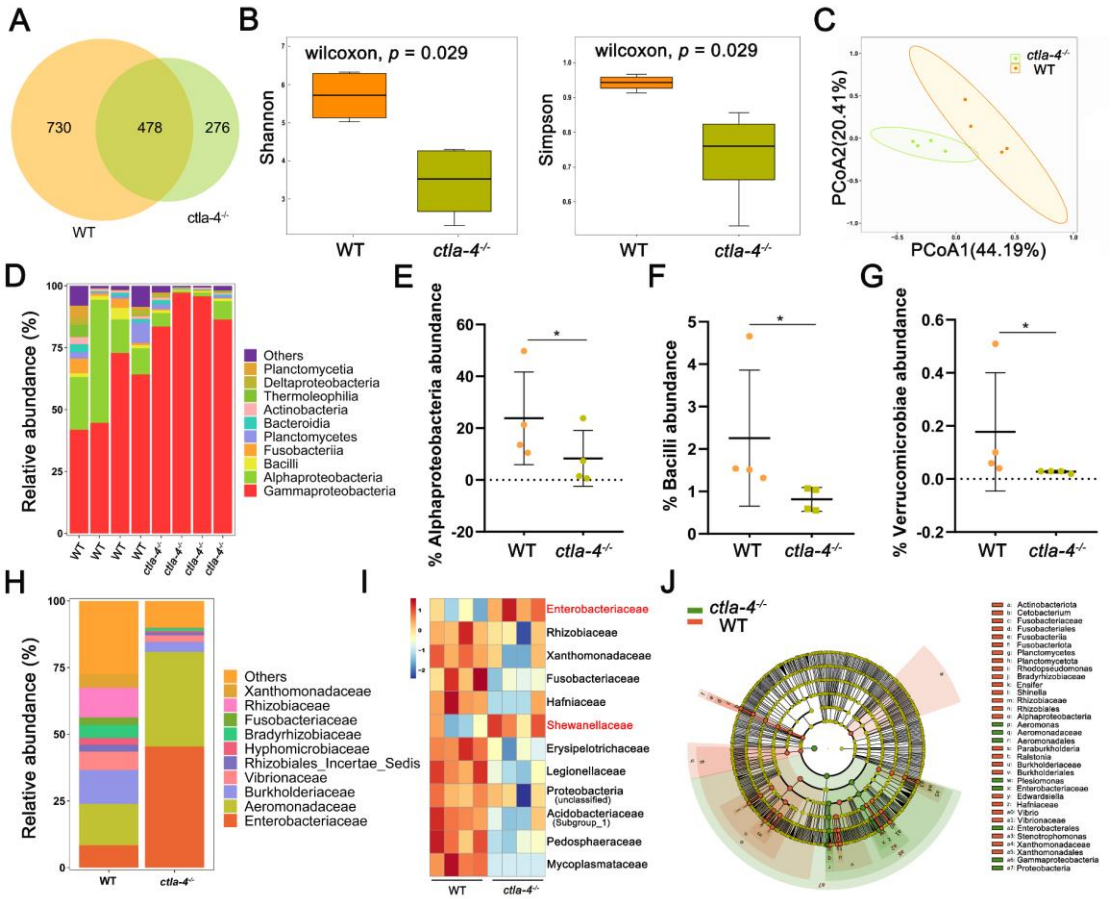

Fig.6 Alteration in microbial composition in the intestines of *ctla-4*$^{-/-}$ zebrafish. **A** Venn diagram showing the number of ASVs in zebrafish intestinal microbiota. **B** Alpha-diversity of microbes was calculated through Shannon index and Simpson index. **C** Beta-diversity analyzed based on PCoA was shown by using Bray Curtis distance. **D** The relative abundance of intestinal microbiota at the class level. **E-G** The relative abundance of Alphaproteobacteria (**E**), Bacilli (**F**) and verrucomicrobiae (**G**) in the intestines from the wild-type (WT) and *ctla-4*$^{-/-}$ zebrafish. $^{*}p < 0.05$. **H** The relative abundance of intestinal microbiota at the family level. **I** Heatmap showing row-scaled expression of the differential abundances of bacterial communities at family level in the WT and *ctla-4*$^{-/-}$ zebrafish ($p < 0.05$). **J** Cladogram representation of LEfSe analysis showing the differentially abundant bacterial taxa between the intestines from WT (red)

and *ctla-4*$^{-/-}$ (green) zebrafish ($p < 0.05$).

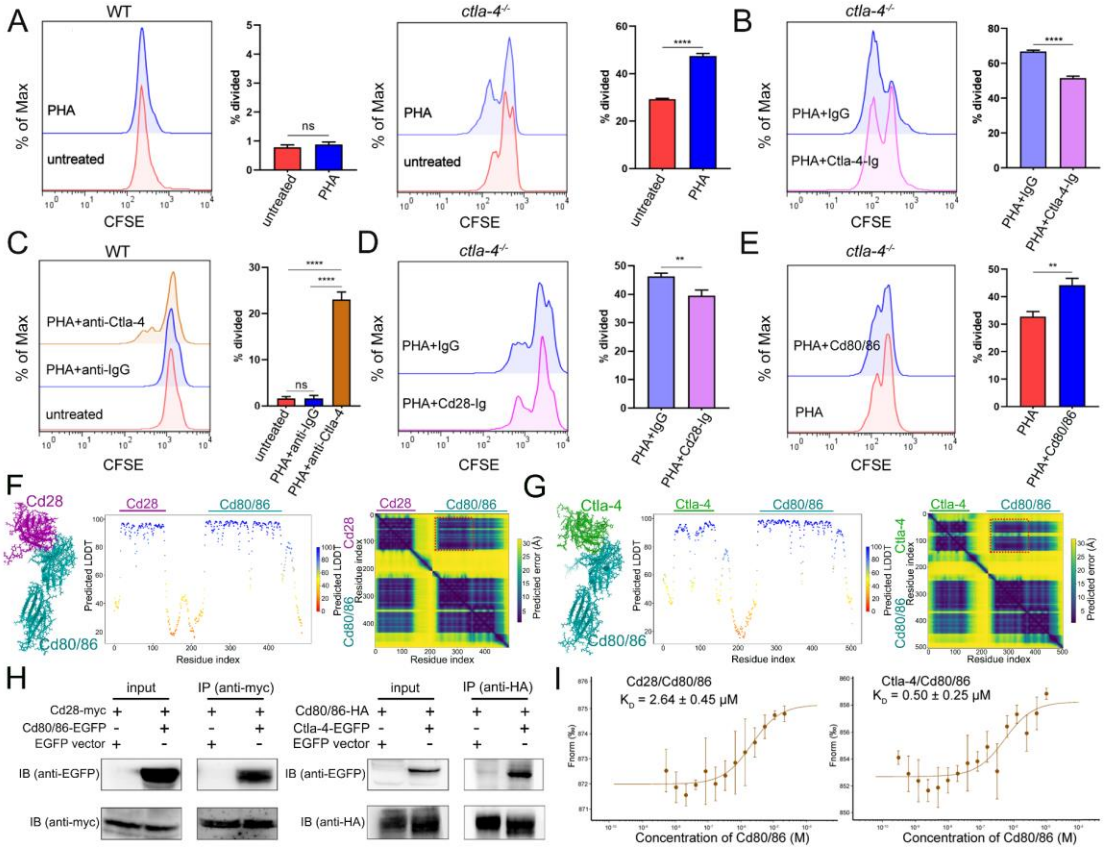

Fig.7 Examination on the inhibitory function of Ctla-4 in T cell activation. **A** Assessment of the proliferative activity of T cells from wild-type (WT) and *ctla-4*$^{-/-}$ zebrafish by a mixed lymphocyte reaction combined with PHA-stimulation. The CFSE dilution, which served as an indicator of lymphocyte proliferation, was measured through flow cytometry. **B** Assessment of the proliferative activity of lymphocytes from *ctla-4*$^{-/-}$ zebrafish by the administration of sCtla-4-Ig. **C** Assessment of the proliferative activity of lymphocytes from WT zebrafish by supplementing anti-Ctla-4 antibody. **D** Assessment of the proliferative activity of lymphocytes from *ctla-4*$^{-/-}$ zebrafish by the administration of sCd28-4-Ig. **E** Assessment of the proliferative activity of lymphocytes

from *ctla-4*$^{-/-}$ zebrafish by the administration of recombinant sCd80/86 protein. **F, G** Interactions between Cd80/86 and Cd28 (**F**), and Cd80/86 and Ctla-4 (**G**) as predicted by AlphaFold2. On the left are structural models depicting Cd80/86 in complex with Cd28 or Ctla-4. The center panels display per-residue model confidence scores (pLDDT) for each structure, using a color gradient from 0 to 100, where higher scores indicate increased confidence. The right panels show the predicated aligned error (PAE) scores for each model. The well-defined interfaces between Cd28 or Ctla-4 and Cd80/86 are highlighted with red dashed squares. **H** The interaction between Cd80/86 and Cd28 (left), and Cd80/86 and Ctla-4 (right) were verified by Co-IP. **I** Binding affinities of the Cd80/86 protein for the Cd28 and Ctla-4 proteins were measured by the microscale thermophoresis (MST) assay. The K_D values are provided. Data are presented as mean ± standard deviation (SD), which were calculated from three independent experiments. Statistical significance was assessed through an unpaired Student's t test ($^{**}p < 0.01$; $^{***}p < 0.001$; ns denotes no statistical significance).

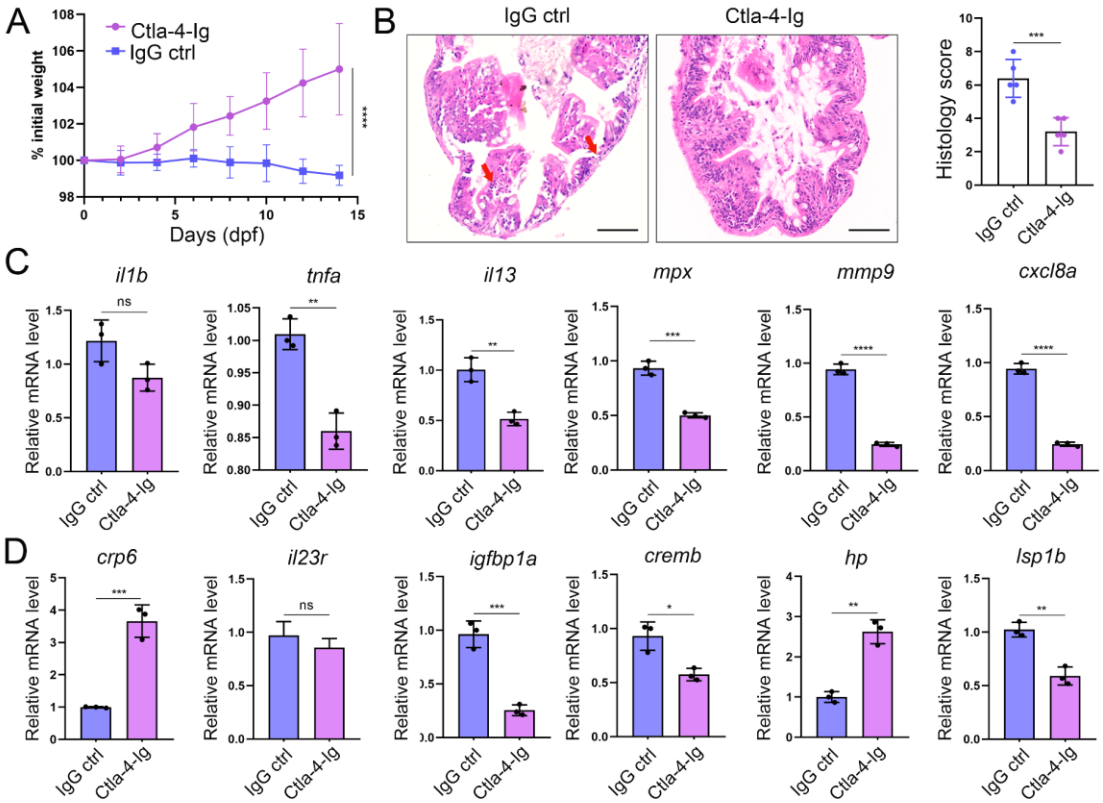

Fig.8 In vivo inhibition of intestinal inflammation by sCtla-4-Ig. **A** Percent initial weight of zebrafish after injection of the sCtla-4-Ig or the IgG isotype control. Each group consisted of six zebrafish (n = 6). Data show means with SEM analyzed by two-way ANOVA with Sidak's correction for multiple comparisons. **B** Representative H&E staining analysis of histopathological changes and quantitation of histology scores in the posterior intestine from *ctla-4*$^{-/-}$ zebrafish treated with sCtla-4-Ig or IgG isotype control. Scale bar: 50 μm. **C** The mRNA expression levels of inflammation-related genes in *ctla-4*$^{-/-}$ zebrafish treated with sCtla-4-Ig or IgG isotype control. **D** The mRNA expression levels of IBD biomarker genes and IBD-related genes in *ctla-4*$^{-/-}$ zebrafish treated with sCtla-4-Ig or IgG isotype control. The *p* value was generated by unpaired two-tailed Student's *t-test*. $^{**}p < 0.01$; $^{***}p < 0.001$; $^{****}p < 0.0001$.

Supplemental Figures

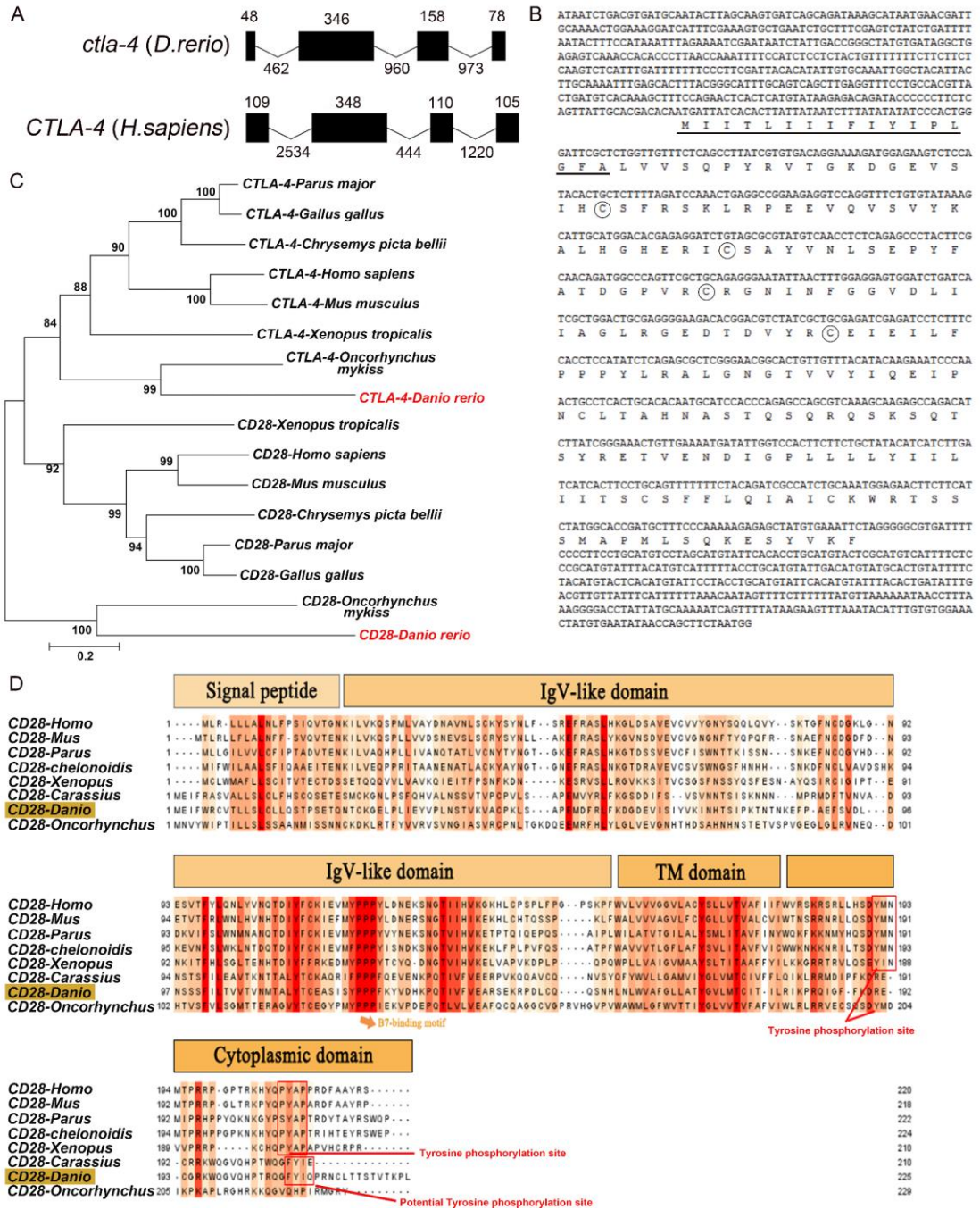

Fig. S1 The organization, sequence and phylogenetic analysis of zebrafish *ctla-4* and *cd28* genes. **A** Comparison of the intron/exon organizations of *ctla-4* gene in zebrafish and humans. Exons and introns are shown with black boxes and lines, and their size are indicated by the numbers found above and below the sequences respectively. **B** The

nucleotide and amino acid sequences of *ctla-4* gene and Ctla-4 protein. The underline indicates the signal peptide, the circles represent the conserved cysteine residues. **C** Phylogenetic analysis of the relationship of Ctla-4 and Cd28 between zebrafish and other species. An unrooted phylogenetic tree was constructed through the neighbor-joining method, based on amino acid sequence alignments generated by ClustalX. Bootstrap confidence values, derived from 500 replicates, are indicated as percentages at each node. **D** Alignment of the Cd28 homologs from different species generated with ClustalX and Jalview. The conserved and partially conserved amino acid residues in each species are colored in hues graded from orange to red, respectively. The conserved functional motifs, such as B7-binding motif, tyrosine phosphorylation site, and potential tyrosine phosphorylation site, were indicated separately. The signal peptide, IgV-like domain, transmembrane (TM) domain and cytoplasmic domain were marked at the top of the sequence.

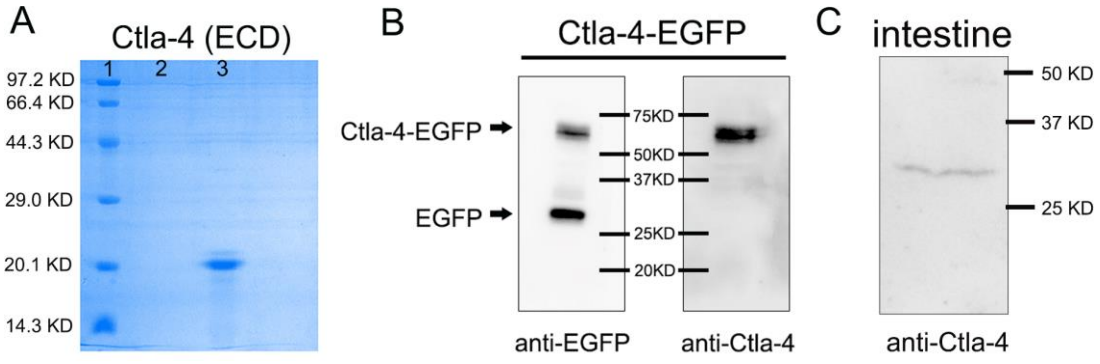

Fig. S2 Preparation of mouse anti-Ctla-4 antibody. **A** SDS-PAGE detection of the recombinant Ctla-4 protein with extracellular domain (ECD). Lane 1, 2 and 3 represent the protein markers, blank, and target protein, respectively. **B** Western blot analysis of

the mouse anti-EGFP and anti-Ctla-4 antibodies that bind to the recombinant Ctla-4-EGFP fusion proteins expressed in HEK293T cells. **C** Western blot analysis of native Ctla-4 protein in zebrafish intestinal tissues using mouse anti-Ctla-4 antibody.

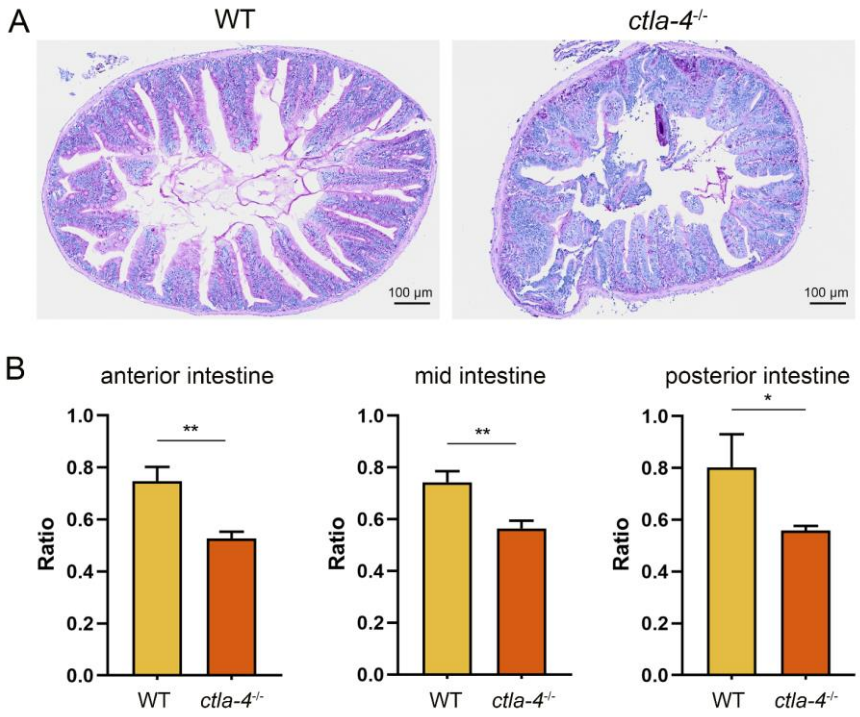

Fig. S3 Histopathological analysis of intestines. **A** Periodic Acid-Schiff (PAS) staining was used to analyze the mucin components in anterior intestine from wild-type (WT) and *ctla-4*$^{-/-}$ zebrafish (n = 5). **B** The ratio of intestinal villi length to intestinal ring radius was measured in the anterior, mid, and posterior intestines of WT and *ctla-4*$^{-/-}$ zebrafish (n = 6). Statistical significance was assessed through an unpaired Student's t test ($^{*}p < 0.05$; $^{**}p < 0.01$).

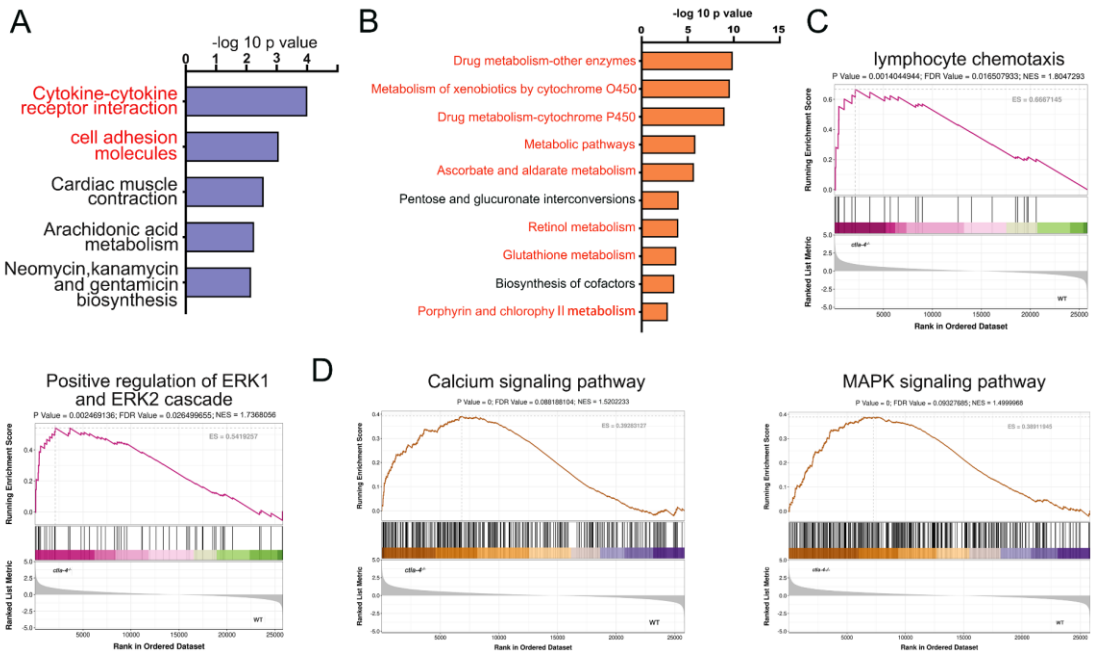

Fig. S4 Examination on the functional genes and pathways associated with the IBD-like phenotype in *ctla-4*$^{-/-}$ zebrafish. **A** Top 5 KEGG enrichment bar plot of up-regulated genes in *ctla-4*$^{-/-}$ zebrafish intestines versus wild-type (WT) zebrafish intestines. **B** Top 10 KEGG enrichment bar plot of down-regulated genes in *ctla-4*$^{-/-}$ zebrafish intestines versus WT zebrafish intestines. **C, D** Changes in the expression of genes associated with lymphocyte chemotaxis, positive regulation of ERK1/ERK2 cascades, Calcium and MAPK signaling pathways in the *ctla-4*$^{-/-}$ zebrafish intestines analyzed by using a collection of pre-defined gene sets retrieved from GO (**C**) and KEGG (**D**) database. The *p* value, false discovery rates (FDR) and normalized enrichment score (NES) are shown above each pathway graph.

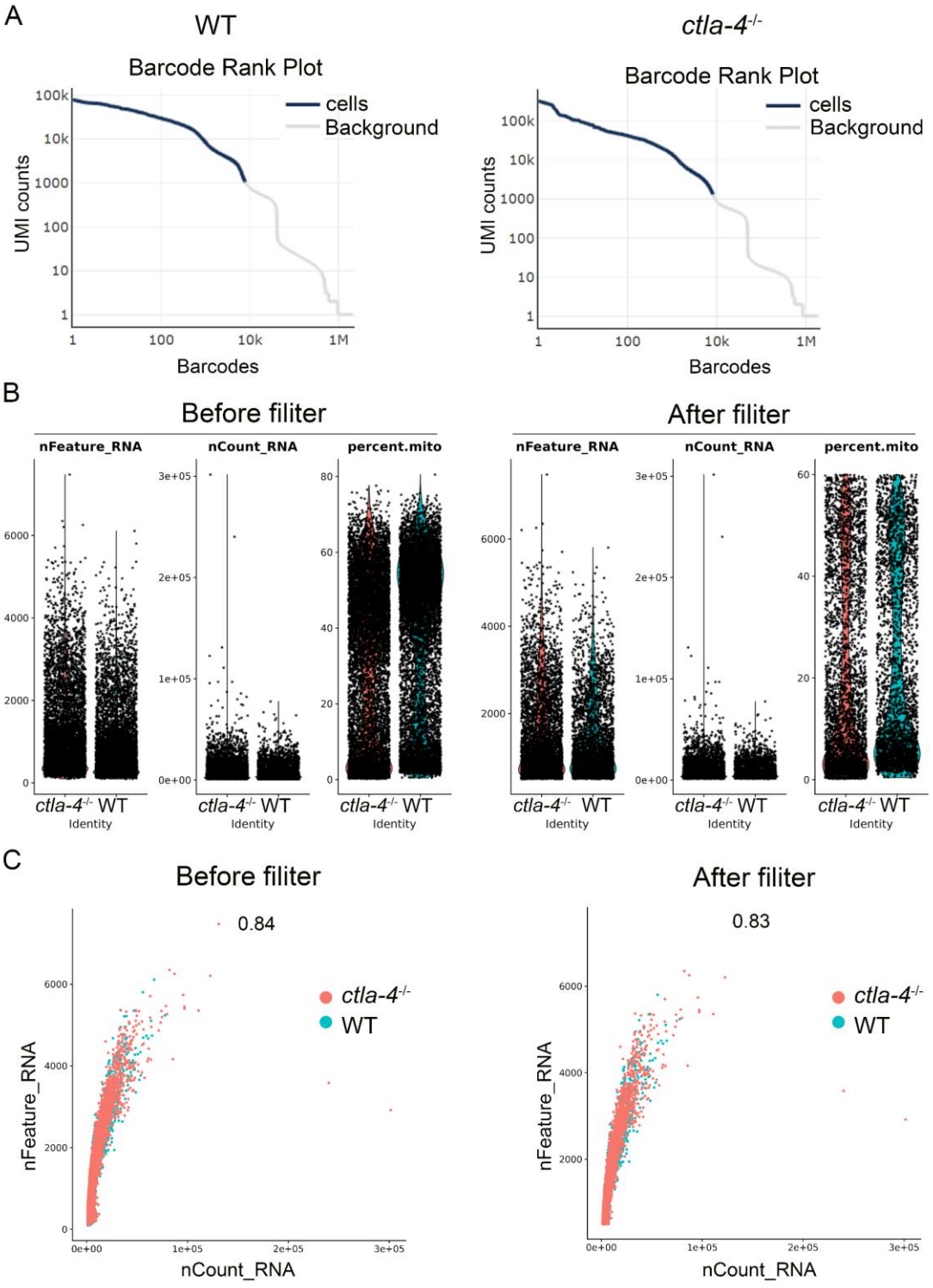

Fig. S5 Quality control analysis of single-cell RNA sequencing data. **A** Identification of the effective cell number of the sample. The blue line represents the effective cells corresponding to barcodes, while the gray line denotes the background noise. **B** The

basic cellular metrics before and after filtering, including the total number of detected genes (nFeature_RNA), the total number of UMIs (nCount_RNA), and the percentage of reads mapped to mitochondrial genes (Percent.mito). **C** The scatter plot comparing the cellular metrics before and after filtering, showing the relationship between nCount_RNA and nFeature_RNA. The Pearson correlation coefficients are indicated above the graph.

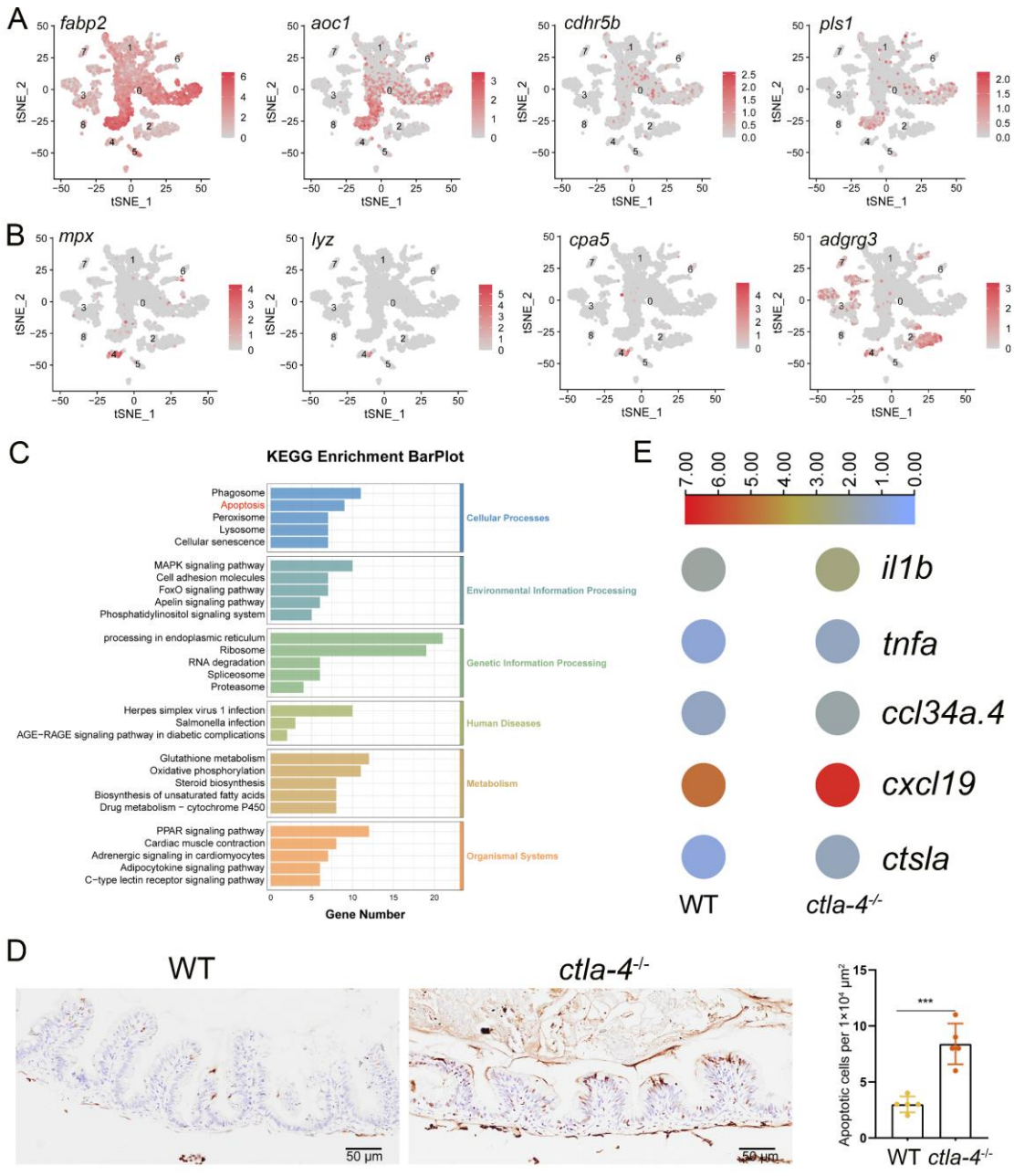

Fig. S6 Examination on the involvement of apoptotic process in epithelial cells and expression of inflammation-related genes in neutrophils and B cells in the intestines of *ctla-4*$^{-/-}$ zebrafish. **A** Expression map of the epithelial markers within the cell populations of the zebrafish intestines. **B** Expression map of the neutrophil markers within the cell populations of the zebrafish intestines. **C** KEGG enrichment bar plot of all differentially expressed genes (DEGs) from epithelial cells. **D** Quantification of TUNEL-positive cells per 1×10^4 μm^2 in WT and *ctla-4*$^{-/-}$ posterior intestines (n = 5). **E** Heatmap of inflammation-related genes in B cells from wild-type and *ctla-4*$^{-/-}$ intestines. Statistical significance was assessed through an unpaired Student's t test (***$p < 0.001$).

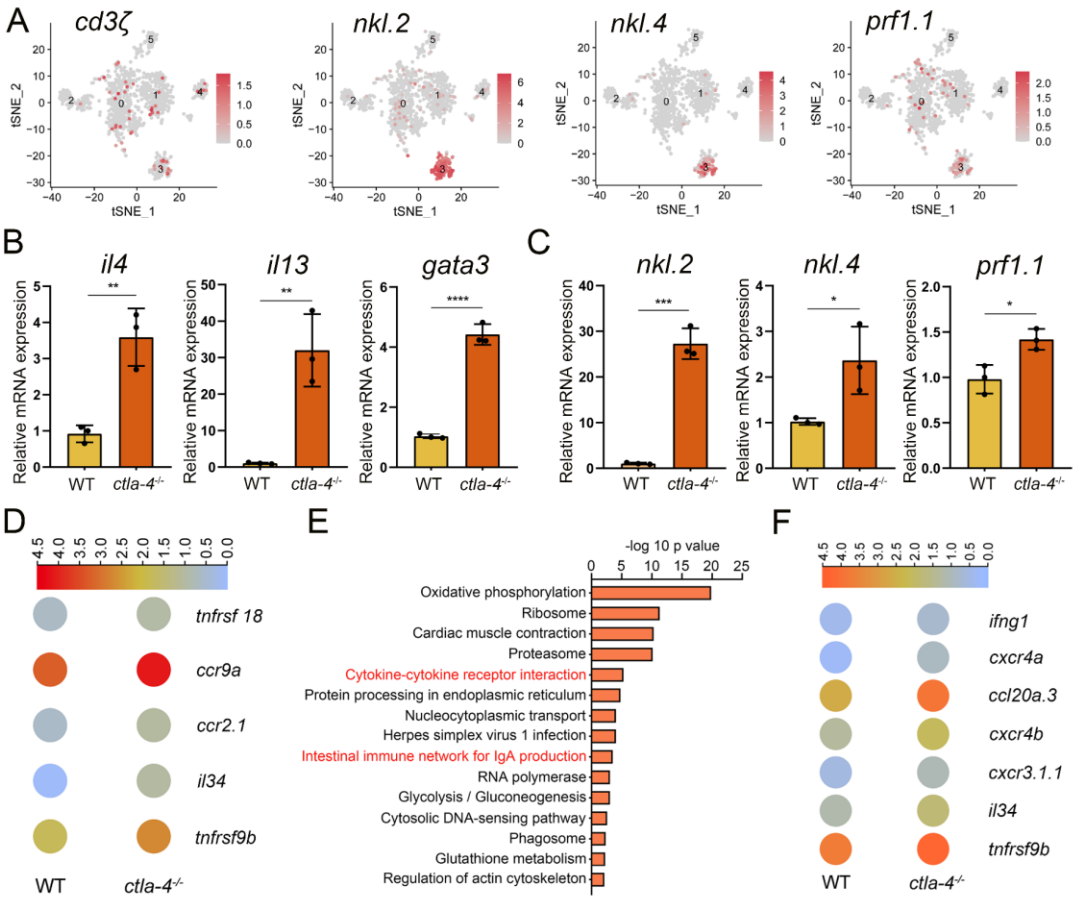

Fig. S7 Examination on the activation of T cell subsets in the intestines of *ctla-4*$^{-/-}$ zebrafish. **A** Marker gene expression in individual cluster identifies the cluster as NKT-like cells. **B** RT-qPCR confirms the mRNA expression levels of Th2 cell marker genes in the intestines of wild-type (WT) and *ctla-4*$^{-/-}$ zebrafish. **C** RT-qPCR validates the mRNA expression levels of NKT-like cell marker genes in the intestines of WT and *ctla-4*$^{-/-}$ zebrafish. **D** Heatmap illustrates up-regulated genes involved in cytokine-cytokine receptor interaction in NKT-like cells from WT and *ctla-4*$^{-/-}$ samples. **E** KEGG enrichment analysis reveals the top 15 terms of up-regulated genes in Cd8^{+} T cells in *ctla-4*$^{-/-}$ samples versus WT samples. **F** Heatmap displays up-regulated genes involved in cytokine-cytokine receptor interaction in Cd8^{+} T cells from WT and *ctla-4*$^{-/-}$ samples. Statistical significance was assessed through an unpaired Student's t test ($^{*}p < 0.05$; $^{**}p < 0.01$; $^{***}p < 0.001$; $^{****}p < 0.0001$).

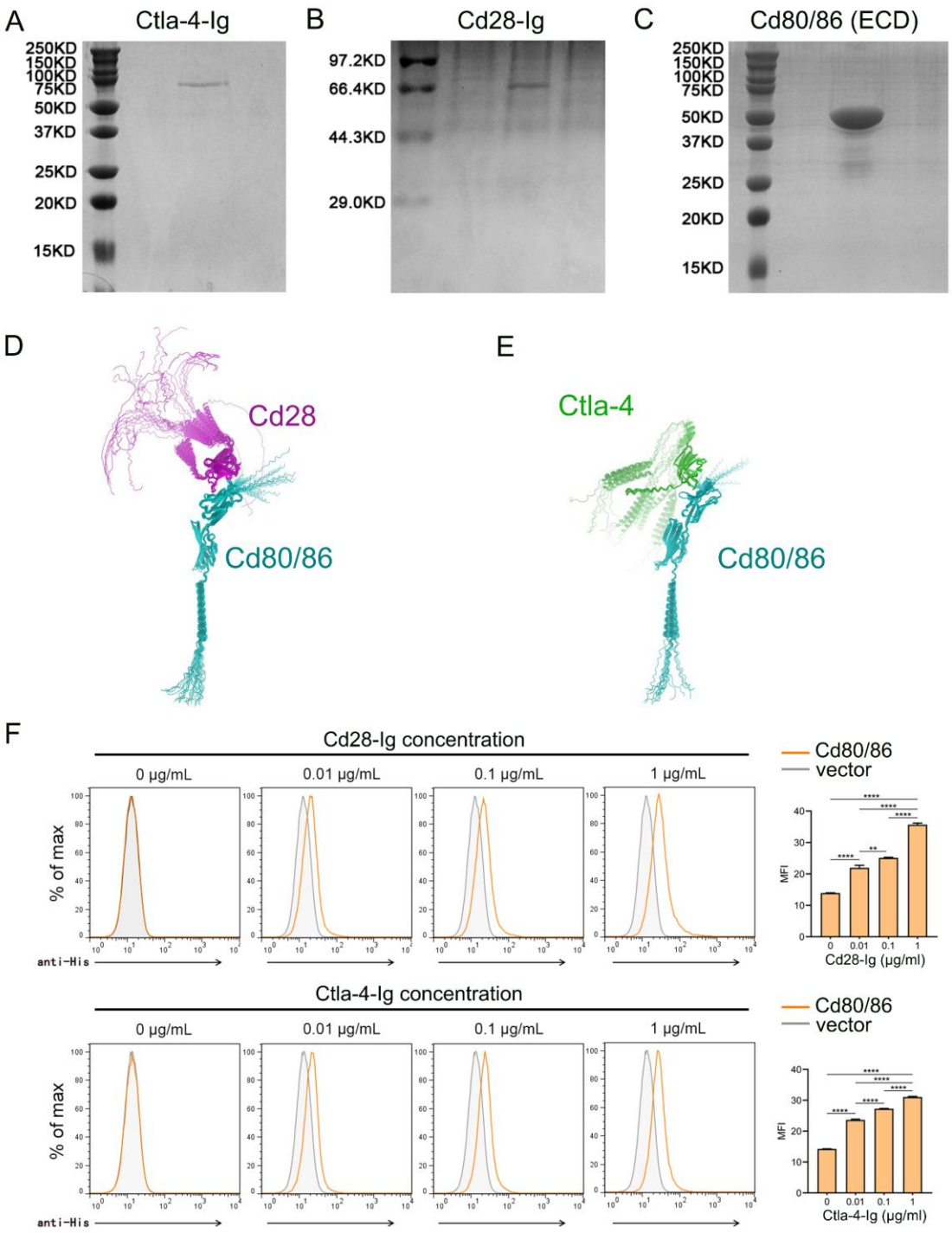

Fig. S8 Preparation of recombinant proteins and examination of their molecular interactions. **A-C** SDS-PAGE detection of the purified recombinant soluble Ctla-4-Ig (sCtla-4) (**A**) and sCd28-Ig (**B**) proteins and the Cd80/86 extracellular domain (ECD) (**C**) with Coomassie brilliant blue staining. **D-E** The predicted molecular interactions

between Cd80/86 and Cd28 (D), as well as Cd80/86 and Ctla-4 (E), as modeled by AlphaFold2. The structures are represented in a cartoon style, with Cd80/86, Cd28, and Ctla-4 colored cyan, green, and magenta, respectively. A total of 25 models were predicted for each complex and aligned with Cd80/86. **F** Flow cytometry analysis of the interactions between Cd80/86 and Cd28 (top), and Cd80/86 and Ctla-4 (bottom). Cd80/86 was expressed on HEK293T cells and incubated with varying concentrations of fluorescently labeled sCd28-Ig or sCtla-4-Ig. Fluorescence intensity was detected by flow cytometry to determine molecular interactions. Data are presented as mean ± SD, derived from three independent experiments. Statistical significance was evaluated using an unpaired Student's t test ($^{**}p < 0.01$; $^{***}p < 0.001$).